Jagiellonian University

Faculty of Physics, Astronomy and Applied Computer Science

Doctoration thesis

Muon capture on the deuteron and ^{3}He

Author:
AlaaEldeen Elmeshneb

Supervisor:
Prof. Jacek Golak

A thesis submitted in fulfilment of the requirements
for the degree of Doctor of Philosophy

in the

March 2015

Declaration of Authorship

I, AlaaEldeen Elmeshneb declare that this thesis titled, ' Muon capture on the deuteron and ^{3}He ' and the work presented in it are my own. I confirm that:

Signed: _____

Date: _____

JAGIELLONIAN UNIVERSITY

Abstract

Faculty of Physics, Astronomy and Applied Computer Science
Marian Smoluchowski Institute of Physics

Doctor of Philosophy

Muon capture on the deuteron and ^{3}He

by AlaaEldeen Elmeshneb

The $\mu^- + ^2\mathrm{H} \to \nu_\mu + n + n$, $\mu^- + ^3\mathrm{He} \to \nu_\mu + ^3\mathrm{H}$, $\mu^- + ^3\mathrm{He} \to \nu_\mu + n + d$, and $\mu^- + ^3\mathrm{He} \to \nu_\mu + n + n + p$ capture reactions are studied using a consistent momentum space framework with various realistic potentials. As a first step, we test our calculation in the case of the $\mu^- + ^2\mathrm{H} \to \nu_\mu + n + n$ and $\mu^- + ^3\mathrm{He} \to \nu_\mu + ^3\mathrm{H}$ reactions, for which theoretical predictions obtained in a comparable framework are available. For these two reactions we obtain results with two-nucleon contributions (meson exchange currents) in the weak current operator, consistent with the AV18 nucleon-nucleon potential. Also for these two reactions we present brand new results based on the recently published improved chiral potentials from the Bochum-Bonn group. Break-up channels in muon capture on ^{3}He are treated under full inclusion of final state interactions, using the framework developed originally for various channels in electron induced break-up of ^{3}He and photodisintegrations reactions. For the sake of completeness we present first basic elements of this formalism. The presented results for the two- and three-body break-up of ^{3}He are calculated with a variety of nucleon-nucleon potentials, among which is the AV18 potential, augmented by the Urbana IX three-nucleon potential. In these calculations only the single nucleon contributions to the weak current operator are retained. We end by recalling the first realistic estimates for the total rates of the muon capture reactions on ^{3}He in the $n + d$ and $n + n + p$ break-up channels.

Acknowledgements

I would like to thank my supervisor, Prof. **Jacek Golak**, for the patient guidance, encouragement and advice he has provided throughout my time as his student. I have been extremely lucky to have a supervisor who cared so much about my work, and who responded to my questions and queries so promptly.

I would also like to thank all the members of staff at Marian Smoluchowski Institute of Physics who helped me in PhD period. In particular I would like to thank Dr. **Roman Skibiński** for the suggestion and help. I will not forget the help and hints of my friend Dr. **Kacper Topolnicki**.

I would like to thank Prof. Laura Marcucci from the University of Piza for sharing her expertise on the weak nuclear current operator and providing me with her numerical results.

I would like to thank Prof. **Evgeny Epelbaum** from the Ruhr-University Bochum for providing me with the computer programs for the new improved chiral potentials and Dr. **Andreas Nogga** from the Jülich Research Center for sending me the ^{3}He and ^{3}H wave functions calculated with various three-nucleon Hamiltonians.

Finally, I would like to thank Dr. **Dagmara Rozpędzik** for technical help in writing two appendices.

Contents

List of Figures

List of Tables

Physical Constants

Neutron mass	M_n	=	939.565	MeV
Proton mass	M_p	=	938.272	MeV
Muon mass	M_μ	=	105.658	MeV
Deuteron mass	M_d	=	1875.612	MeV
Fine structure constant	α	=	$1/137.0359$	$Dimensionless$
Fermi coupling constant	G	=	1.14939×10^{-5}	GeV^{-2}
Speed of Light	c	=	$29.9792458 \times 10^{22}$	fm/s
Conversion constant	$\hbar c$	=	197.327	$MeV.fm$

Symbols

l	Two nucleon orbital angular momentum
s	Two nucleon spin angular momentum
t	Two nucleon isospin angular momentum
j	Two nucleon total angular momentum
$2N$	Two nucleon system
$3N$	Three nucleon system

Dedicated to: my Parents, Wife and Children (Mohamed and Jasmine)

Chapter 1

Introduction

The history of our understanding of the weak force is very long and full of unexpected realizations [1]. It starts with Henri Becquerel's discovery of radioactivity in 1896 and subsequent classification of radioactivity into alpha, beta and gamma decays of the nucleus by Ernest Rutherford and others. Among those, Maria Skłodowska-Curie and Pierre Curie's pioneering research should be gratefully acknowledged.

Enrico Fermi formulated the first theory for the beta-decay process in 1934. He was inspired by Quantum Electrodynamics and Wolfgang Pauli's suggestion that along with the electron, a very light neutral particle was also emitted in his experiment. Many years of both theoretical and experimental efforts have brought us to the present-day picture of the weak interactions. A more complete discussion is beyond the scope of this thesis but we would like to draw the reader's attention to two papers published in the Cornell University Library Archive [2, 3], since they offer a short but quite informative introduction to the subject. In particular, the following list of "milestones in the history of weak interactions"from Ref. [3] is worth citing:

1896 Discovery of radioactivity (Becquerel)
1930 Birth of neutrino (Pauli)
1934 Theory of beta decay (Fermi)
1939 Theory of thermonuclear fusion in the Sun (Bethe and von Weizsäcker)
1954 Nonabelian gauge theory (Yang and Mills)
1956 Discovery of parity violation (Lee, Yang and Wu)
1956 Detection of the neutrino (Cowan and Reines)
1957 Discovery of V-A (Sudarshan, Marshak and others)
1957 Current $\times$ current formulation (Feynman and Gell-Mann)
1961 SU(2) $\times$ U(1) as the electroweak group (Glashow)
1964 Discovery of CP violation (Cronin and Fitch)

1964 Abelian Higgs mechanism (Higgs and others)
1967 Nonabelian Higgs-Kibble mechanism (Kibble)
1967 Electroweak theory (Salam and Weinberg)
1972 Renormalizability of EW theory (t'Hooft and Veltman)
1973 Discovery of neutral current (55 physicists at CERN)
1973 CKM phase for CP violation (Kobayashi and Maskawa)
1982 Discovery of W and Z (Rubbia and Van der Meer)
1992 Precision tests of EW theory (International Collaboration at CERN)
1998 Discovery of neutrino mass (Davis, Koshiba and others)
2002 Experimental proof of thermonuclear fusion in the Sun (SNO)
2007 Verification of CKM theory of CP violation (KEK, Stanford)
2012 Discovery of Higgs boson (ATLAS and CMS Collaborations, CERN)

So we now know that no weak processes involving nucleons can be regarded as being truly "elementary"and that nucleons are only the effective (and in fact very efficient) degrees of freedom for low-energy nuclear reactions. Muon capture on the proton, $\mu^- + p \to \nu_\mu + n$, is a perfect example of such a process. In its description, the complete knowledge about the muon current must be combined with the imperfect knowledge about the weak current of the nucleon, turning the proton into the neutron. Thus this reaction couples information from the neutron beta decay and the muon decay reactions.

Muon capture reactions on light nuclei have been studied intensively both experimentally and theoretically for many years. As for the details of the physics motivation in the particular case of the $\mu^- + {}^2\mathrm{H} \to \nu_\mu + n + n$ capture reaction we refer the reader to the web page of the MuSun experiment [4], which aims to measure the capture rate from the doublet hyperfine state of the muonic deuterium atom in its ground state to a precision of better than 1.5 %. Here we repeat only after [4] that

1. Muon capture on the deuteron is the simplest weak interaction process on a nucleus which can both be calculated and measured to a high degree of precision.

2. This reaction is closely related to fundamental reactions of astrophysical interest, in particular to the $p + p \to d + e^+ + \bar{\nu}_e$ process.

3. In the effective field theory approaches this reaction is linked to other physics.

For information on earlier achievements we refer the reader to Refs. [5–7]. More recent theoretical work, focused on the $\mu^- + {}^2\mathrm{H} \to \nu_\mu + n + n$ and $\mu^- + {}^3\mathrm{He} \to \nu_\mu + {}^3\mathrm{H}$ reactions, has been summarized in Refs. [8, 9]. Here we mention only that the calculation of Ref. [8], following the early steps of Ref. [10], was performed both in the phenomenological and

the "hybrid" chiral effective field theory (χEFT) approach. In the first approach, Hamiltonians based on conventional two-nucleon (2N) and three-nucleon (3N) potentials were used to calculate the nuclear wave functions, and the weak transition operator included, beyond the single nucleon contribution associated with the basic process $\mu^- + p \to \nu_\mu + n$, meson-exchange currents as well as currents arising from the excitation of Δ-isobar degrees of freedom [11]. In the hybrid χEFT approach, the weak operators were derived in χEFT, but their matrix elements were evaluated between wave functions obtained from conventional potentials. Typically, the potential model and hybrid χEFT predictions are in good agreement with each other [8]. Only very recently, the two reactions have been studied in a "non-hybrid" χEFT approach [12], where both potentials and currents are derived consistently in χEFT and the low-energy constants present in the 3N potential and two-body axial-vector current are constrained to reproduce the $A = 3$ binding energies and the Gamow-Teller matrix element in tritium β-decay. An overall agreement between the results obtained within different approaches has been found, as well as between theoretical predictions and available experimental data.

The first theoretical study for the capture $\mu^- + {}^3\mathrm{He} \to \nu_\mu + n + d$ was reported in Ref. [13]. A simple single nucleon current operator was used without any relativistic corrections and the initial and final 3N states were generated using realistic nucleon-nucleon potentials but neglecting the 3N interactions.

In the recent paper [14] attempts to use the momentum space treatment of electromagnetic processes from [15, 16] and the potential model approach developed in Ref. [8] were joined to perform a systematic study of all the $A = 2$ and $A = 3$ muon capture reactions, extending the calculations of Ref. [13] to cover also the $\mu^- + {}^3\mathrm{He} \to \nu_\mu + n + n + p$ channel. The results obtained for the $\mu^- + {}^2\mathrm{H} \to \nu_\mu + n + n$ and $\mu^- + {}^3\mathrm{He} \to \nu_\mu + {}^3\mathrm{H}$ reactions using the Faddeev equations in the momentum space were compared with those of Ref. [8], obtained using the hyperspherical harmonics formalism (for a review, see Ref. [17]). In [14] predictions for the total and differential capture rates of the reactions $\mu^- + {}^3\mathrm{He} \to \nu_\mu + n + d$ and $\mu^- + {}^3\mathrm{He} \to \nu_\mu + n + n + p$, obtained with full inclusion of final state interactions, employing not only nucleon-nucleon but also 3N forces, were presented. Note that the bulk of the results in [14] was calculated with the single nucleon current operator.

In this thesis we incorporate to a large extent the results from [14] but add also new ingredients. First of all, we supplement our weak current operator with two-nucleon contributions. Although not all the operators used, for example, in [8] are yet incorporated, we demonstrate that in our framework the so-called meson exchange currents given in the momentum space can be included.

Recently, improved chiral nucleon-nucleon potentials from the Bochum-Bonn group [18] appeared. It is very interesting to obtain predictions based on this new nucleon-nucleon force, which is now available to us at different orders of the chiral expansion (from the lowest order up to even next-to-next-to-next-to-next-to leading order). This set of potentials is going to be widely used to solve the structure and reactions of light and heavier nuclei. So far no current operator consistent with this set of nucleon-nucleon potentials has been constructed, so the calculations are performed with the single nucleon current operator. In the thesis we present results based on this new type of chiral forces for the $\mu^- + {}^2\mathrm{H} \to \nu_\mu + n + n$ and $\mu^- + {}^3\mathrm{He} \to \nu_\mu + {}^3\mathrm{H}$ reactions. Our results demonstrate some very welcome features; for example the range of predictions obtained with different regulators gets narrower for the higher and higher orders of the chiral expansion.

The thesis is organized in the following way. In Chapter 2 we introduce first the single nucleon current operator, which we treat in momentum space, and compare our expressions with those of Ref. [8]. We show how to efficiently obtain the corresponding matrix elements in the partial wave basis. In the same chapter we list also the two-nucleon contributions to the current operator, given originally in Ref. [11], which will be used in the thesis.

In the following two chapters we show selected results for the $\mu^- + {}^2\,\mathrm{H} \to \nu_\mu + n + n$ (Chapter 3) and for the $\mu^- + {}^3\,\mathrm{He} \to \nu_\mu + {}^3\,\mathrm{H}$ (Chapter 4) reactions. Since in the thesis we use the two-nucleon and three-nucleon partial wave states, we face the non-trivial task to calculate the matrix elements of the single nucleon and two-nucleon current operators. In the corresponding chapters we briefly describe our method and provide the basic expressions.

For the sake of completeness, in Chapter 5 we recapitulate the way we calculate the total capture rates for the two break-up reactions, $\mu^- + {}^3\,\mathrm{He} \to \nu_\mu + n + d$ and $\mu^- + {}^3\,\mathrm{He} \to \nu_\mu + n + n + p$, and show predictions obtained with different 3N dynamics. In these calculations we employ mainly the AV18 nucleon-nucleon potential [19] supplemented with the Urbana IX 3N potential [20].

Chapter 6 contains our summary and conclusions.

The thesis contains also 4 appendices. Appendix A and Appendix B show two simple warm-up exercises, where we calculate the muon and neutron lifetimes. We check in this way our *Mathematica*® [21] tools, which are predominantly used to calculate momentum dependent spin-isospin matrix elements in Chapters 2 and 3.

Appendix C deals with the numerical calculation of the deuteron wave function in the partial wave basis of the momentum space. Finally, Appendix D shows how to obtain the numerical solution of the Lippmann-Schwinger equation.

Chapter 2

Weak current operator

2.1 The single nucleon current operator

In the muon capture process we assume that the initial state $\mid i \rangle$ consists of the atomic K-shell muon wave function $\mid \psi\, m_\mu \rangle$ with the muon spin projection m_μ and the initial nucleus state with the three-momentum $\mathbf{P}_i$ (and the spin projection m_i):

$$\mid i \rangle = \mid \psi\, m_\mu \rangle \mid \Psi_i\, \mathbf{P}_i\, m_i \rangle\,. \tag{2.1}$$

In the final state, $\mid f \rangle$, one encounters the muon neutrino (with the three-momentum $\mathbf{p}_\nu$ and the spin projection m_ν), as well as the final nuclear state with the total three-momentum $\mathbf{P}_f$ and the set of spin projections m_f:

$$\mid f \rangle = \mid \nu_\mu\, \mathbf{p}_\nu\, m_\nu \rangle \mid \Psi_f\, \mathbf{P}_f\, m_f \rangle\,. \tag{2.2}$$

The transition from the initial to final state is driven by the Fermi form of the interaction Lagrangian (see for example Ref. [22]) and leads to a contraction of the leptonic ($\mathcal{L}_\lambda$) and nuclear ($\mathcal{N}^\lambda$) parts in the S-matrix element, S_{fi} [13]:

$$S_{fi} = i(2\pi)^4\, \delta^4\left(P' - P\right) \frac{G}{\sqrt{2}}\, \mathcal{L}_\lambda\, \mathcal{N}^\lambda\,, \tag{2.3}$$

where $G = 1.14939 \times 10^{-5}\,\mathrm{GeV}^{-2}$ is the Fermi constant (taken from Ref. [8]), and P (P') is the total initial (final) four-momentum. The well known leptonic matrix element

$$\mathcal{L}_\lambda = \frac{1}{(2\pi)^3}\, \bar{u}(\mathbf{p}_\nu, m_\nu)\gamma_\lambda(1-\gamma_5)u(\mathbf{p}_\mu, m_\mu) \equiv \frac{1}{(2\pi)^3}\, L_\lambda \tag{2.4}$$

is given in terms of the Dirac spinors (note that we use the notation and spinor normalization of Bjorken and Drell [23]).

The nuclear part is the essential ingredient of the formalism, and is written as

$$\mathcal{N}^{\lambda} = \frac{1}{(2\pi)^3} \langle \Psi_f \, \mathbf{P}_f \, m_f \mid j_w^{\lambda} \mid \Psi_i \, \mathbf{P}_i \, m_i \rangle \equiv \frac{1}{(2\pi)^3} N^{\lambda} \, . \tag{2.5}$$

It is a matrix element of the nuclear weak current operator j_w^{λ} between the initial and final nuclear states. The primary form of N^{λ} is present already in such basic processes (from the point of view of the Fermi theory) as the neutron beta decay or the low-energy $\mu^- + p \to \nu_\mu + n$ reaction. General considerations, taking into account symmetry requirements, lead to the following form of the single nucleon current operator [24], whose matrix elements depend on the nucleon incoming ($\mathbf{p}$) and outgoing momentum ($\mathbf{p}'$) and nucleon spin projections m and m':

$$\begin{aligned} &\langle \frac{1}{2} m' \mid \langle \mathbf{p}' \mid j_w^{\lambda}(1) \mid \mathbf{p} \rangle \mid \frac{1}{2} m \rangle = \\ &\bar{u}(\mathbf{p}', m') \Big(\left(g_1^V - 2M \, g_2^V \right) \gamma^{\lambda} + g_2^V \left(p + p' \right)^{\lambda} \\ &+ g_1^A \gamma^{\lambda} \gamma^5 + g_2^A \left(p - p' \right)^{\lambda} \gamma^5 \Big) \tau_- u(\mathbf{p}, m) \, , \end{aligned} \tag{2.6}$$

containing nucleon weak form factors, g_1^V, g_2^V, g_1^A, and g_2^A, which are functions of the four-momentum transfer squared, $(p' - p)^2$. We neglect the small difference between the proton mass M_p and neutron mass M_n and introduce the average "nucleon mass", $M \equiv \frac{1}{2}(M_p + M_n)$. Working with the isospin formalism, we introduce the isospin lowering operator, as $\tau_- = (\tau_x - \mathrm{i}\tau_y)/2$. Since the wave functions are generated by non-relativistic equations, it is necessary to perform the non-relativistic reduction of Eq. (2.6). The non-relativistic form of the time and space components of $j_w^{\lambda}(1)$ reads

$$\langle \mathbf{p}' \mid j_{\mathrm{NR}}^0(1) \mid \mathbf{p} \rangle = \left(g_1^V + g_1^A \frac{\boldsymbol{\sigma} \cdot (\mathbf{p} + \mathbf{p}')}{2M} \right) \tau_- \tag{2.7}$$

and

$$\begin{aligned} &\langle \mathbf{p}' \mid \mathbf{j}_{\mathrm{NR}}(1) \mid \mathbf{p} \rangle = \\ &\Big(g_1^V \frac{\mathbf{p} + \mathbf{p}'}{2M} - \frac{1}{2M} \left(g_1^V - 2M g_2^V \right) i \, \boldsymbol{\sigma} \times \left(\mathbf{p} - \mathbf{p}' \right) \\ &+ g_1^A \boldsymbol{\sigma} + g_2^A \left(\mathbf{p} - \mathbf{p}' \right) \frac{\boldsymbol{\sigma} \cdot (\mathbf{p} - \mathbf{p}')}{2M} \Big) \tau_- \, , \end{aligned} \tag{2.8}$$

where $\boldsymbol{\sigma}$ is a vector of Pauli spin operators. Here we have kept only terms up to $1/M$.

Very often relativistic $1/M^2$ corrections are also included. This leads then to additional terms in the current operator:

$$\begin{aligned}
&\langle \mathbf{p}\,' \mid j^0_{\rm NR+RC}(1) \mid \mathbf{p}\rangle = \\
&\Big(g_1^V - (g_1^V - 4M g_2^V)\frac{(\mathbf{p}\,'-\mathbf{p}\,)^2}{8M^2} + \big(g_1^V - 4M g_2^V\big)\, i\,\frac{(\mathbf{p}\,'\times\mathbf{p}\,)\cdot\boldsymbol{\sigma}}{4M^2} \\
&+ g_1^A \frac{\boldsymbol{\sigma}\cdot(\mathbf{p}+\mathbf{p}\,')}{2M} + g_2^A \frac{(\mathbf{p}\,'^2 - \mathbf{p}^2)}{4M^2}\boldsymbol{\sigma}\cdot(\mathbf{p}\,'-\mathbf{p}\,)\Big)\tau_-
\end{aligned} \tag{2.9}$$

and

$$\begin{aligned}
&\langle \mathbf{p}\,' \mid \mathbf{j}_{\rm NR+RC}(1) \mid \mathbf{p}\rangle = \\
&\Big(g_1^V \frac{\mathbf{p}+\mathbf{p}\,'}{2M} - \frac{1}{2M}\big(g_1^V - 2M g_2^V\big)\, i\,\boldsymbol{\sigma}\times(\mathbf{p}-\mathbf{p}\,') \\
&+ g_1^A \left(1 - \frac{(\mathbf{p}+\mathbf{p}\,')^2}{8M^2}\right)\boldsymbol{\sigma} + \\
&+ \frac{g_1^A}{4M^2}\big[\,(\mathbf{p}\cdot\boldsymbol{\sigma})\,\mathbf{p}\,' + (\mathbf{p}\,'\cdot\boldsymbol{\sigma})\,\mathbf{p} + i\,(\mathbf{p}\times\mathbf{p}\,')\,\big]) \\
&+ g_2^A\,(\mathbf{p}-\mathbf{p}\,')\,\frac{\boldsymbol{\sigma}\cdot(\mathbf{p}-\mathbf{p}\,')}{2M}\Big)\tau_- \,.
\end{aligned} \tag{2.10}$$

This form of the nuclear weak current operator is very close to the one used in Ref. [8], provided that one term,

$$g_2^V \frac{(\mathbf{p}\,'-\mathbf{p}\,)^2}{2M} \tag{2.11}$$

is dropped in Eq. (2.9) and we use:

$$G_E^V = g_1^V\,, \tag{2.12}$$

$$G_M^V = g_1^V - 2M g_2^V\,, \tag{2.13}$$

$$G_A = -g_1^A\,, \tag{2.14}$$

$$G_P = -g_2^A m_\mu\,. \tag{2.15}$$

Here the form factors G_E^V and G_M^V are the isovector components of the electric and magnetic Sachs form factors, while G_A and G_P are the axial and pseudoscalar form factors. Their explicit expressions and parametrization can be found in Ref. [25]. We also verified that the extra term (2.11) gives negligible effects in all studied observables.

Results in this thesis are obtained solely using the standard partial wave decomposition. The two-nucleon (2N) momentum space partial wave states, $\mid p\bar{\alpha}_2\,\rangle$, carry information about the magnitude of the relative momentum (p), the relative angular momentum (l), spin (s) and total angular momentum (j) with the corresponding projection (m_j) in $\bar{\alpha}_2$.

This set of quantum numbers is supplemented by the 2N isospin (t) and its projection (m_t). We list all the two-neutron partial wave states with $j \leq 6$ in Table 2.1. In order to avoid the cumbersome task of PWD of the many terms in Eqs. (2.9) and (2.10) we proceed in the same way as for the nuclear potentials in the so-called automatized PWD method [26, 27]. In the case of the single nucleon current operator it leads to a general formula

$$\begin{aligned}
&\langle p(ls)jm_j\, tm_t\, \mathbf{P}_f \mid j_w(1) \mid \phi_d\, \mathbf{P}_i\, m_d \rangle \;=\; \delta_{t,1}\, \delta_{m_t,-1} \left\langle 1-1 \mid \tau_-(1) \mid 00 \right\rangle \\
&c\,(l,s,j;m_l,m_j-m_l,m_j\,) \sum_{l_d=0,2} \sum_{m_{l_d}} c\,(l_d,1,1;m_{l_d},m_d-m_{l_d},m_d\,) \\
&\sum_{m_1} c\left(\frac{1}{2},\frac{1}{2},s;m_1,m_j-m_l-m_1,m_j-m_l\right) \\
&\sum_{m_{1_b}} c\left(\frac{1}{2},\frac{1}{2},1;m_{1_b},m_d-m_{l_d}-m_{1_d},m_d-m_{l_d}\right) \\
&\delta_{m_j-m_l-m_1,m_d-m_{l_d}-m_{1_d}} \\
&\int d\hat{\mathbf{p}}\, Y^*_{l\,m_l}\,(\hat{\mathbf{p}})\; Y_{l_d\,m_{l_d}}\left(\widehat{\mathbf{p}-\frac{1}{2}\mathbf{Q}}\right)\; \varphi_{l_d}\left(\mid \mathbf{p}-\frac{1}{2}\mathbf{Q}\mid\right) \\
&\left\langle \frac{1}{2}m_1 \mid \left\langle \mathbf{p}+\frac{1}{2}\mathbf{P}_f \mid j_w^{\rm spin}(1) \mid \mathbf{p}-\frac{1}{2}\mathbf{P}_f+\mathbf{P}_i \right\rangle \mid \frac{1}{2}m_{1_d} \right\rangle
\end{aligned} \tag{2.16}$$

where $\mathbf{Q} \equiv \mathbf{P}_f - \mathbf{P}_i$ and the deuteron state contains two components

$$\mid \phi_d\, m_d \rangle = \sum_{l_d=0,2} \int dpp^2 \;\mid p(l_d 1)1 m_d \rangle \mid 00 \rangle\, \varphi_{l_d}\,(p)\;. \tag{2.17}$$

Using software for symbolic algebra, for example *Mathematica*® [21], we easily prepare momentum dependent spin matrix elements

$$\left\langle \frac{1}{2}m' \mid \left\langle \mathbf{p}_1{}' \mid j_w^{\rm spin}(1) \mid \mathbf{p}_1 \right\rangle \mid \frac{1}{2}m \right\rangle \tag{2.18}$$

for any type of the single nucleon operator.

Some examples of the resulting $\langle p(ls)jm_j\, tm_t\, \mathbf{P}_f \mid j_w(1) \mid \phi_d\, \mathbf{P}_i\, m_d \rangle$ matrix elements are given in Figs. 2.3–2.6. It is clear that for the two-neutron system we have $t = 1$ and $m_t = -1$. Further, we calculate these matrix elements for $\mathbf{P}_i = 0$ and for $\mathbf{P}_f$ parallel to the z-axis. This yields a simple relation between m_d and m_j: For the density matrix elements (denoted as N_0) and for the z Cartesian component of the vector current (N_z) it holds that $m_j = m_d$. For the -1 spherical component of the vector current (N_{-1}) thus results in $m_j = m_d - 1$. Such a choice means that the magnitude of the three momentum transfer $\mid \mathbf{P}_f - \mathbf{P}_i \mid$ is equal to the energy of the outgoing neutrino E_ν. (We adopt in the thesis the natural system of units, where $c = \hbar = 1$.)

TABLE 2.1: The two-nucleon partial wave states used in the calculations of the $\mu^- + {}^2\mathrm{H} \to \nu_\mu + n + n$ reaction up to the total angular momentum $j_{max} = 6$. The total two-nucleon isospin is $t = 1$.

2N partial wave ($\bar{\alpha}_2$)	l	s	j
1	0	0	0
2	1	1	0
3	1	1	1
4	2	0	2
5	1	1	2
6	3	1	2
7	3	1	3
8	4	0	4
9	3	1	4
10	5	1	4
11	5	1	5
12	6	0	6
13	5	1	6
14	7	1	6

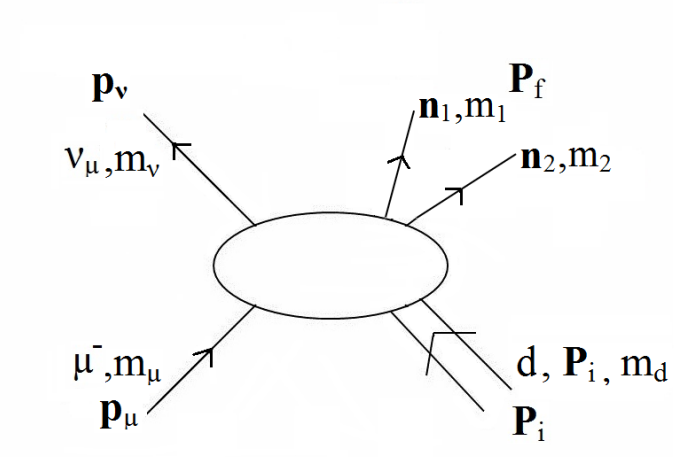

FIGURE 2.1: General diagram for muon capture on the deuteron. The details of the lepton-nucleus interaction are hidden inside the ellipse.

For the six dominant partial wave states we show two sets of figures, at two different neutrino energies. Clearly shapes of the lines change with this energy, especially for the higher partial waves.

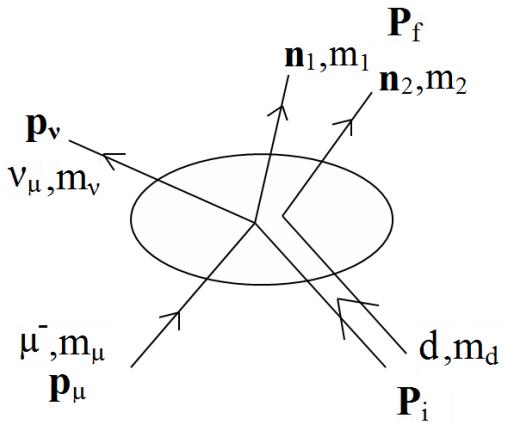

FIGURE 2.2: Diagram representing the single nucleon current operator. Note that the lepton line is attached only to nucleon 1.

2.2 Two-body current operators

It is clear that on top of the single nucleon operators, also many-nucleon contributions appear in j^λ_w. In the 3N system one can even expect 3N current operators:

$$j^\lambda_w = j^\lambda_w(1) + j^\lambda_w(2) + j^\lambda_w(3) + j^\lambda_w(1,2) + j^\lambda_w(1,3) + j^\lambda_w(2,3) + j^\lambda_w(1,2,3)\,. \qquad (2.19)$$

The role of these many-nucleon operators has been studied for example in Ref. [8].

In this section we discuss, very briefly, our approach to the two-body weak current. The construction of current operators that are entirely consistent with a given model of nuclear forces is very difficult. Several attempts have been made, especially in the framework of the chiral effective field theory (see for example [8]), but none of them is fully satisfactory.

In our thesis we rely on the experience of the Pisa group and use the expressions from [11]. That paper provides formulas for the two-body weak current operators to be used with the well established AV18 nucleon-nucleon potential [19].

Like the one-body current, also two-body nuclear weak current consists of vector and axial-vector parts. The weak vector current is constructed from the isovector part of the electromagnetic current, in accordance with the conserved-vector-current (CVC) hypothesis. Two-body weak vector currents have terms which are obtained from the nucleon-nucleon interaction and are called "model-independent"(MI). There are also "model-dependent"(MD) contributions that cannot be linked (via the continuity equation) to the nucleon-nucleon potential. The most important two-body weak vector MI

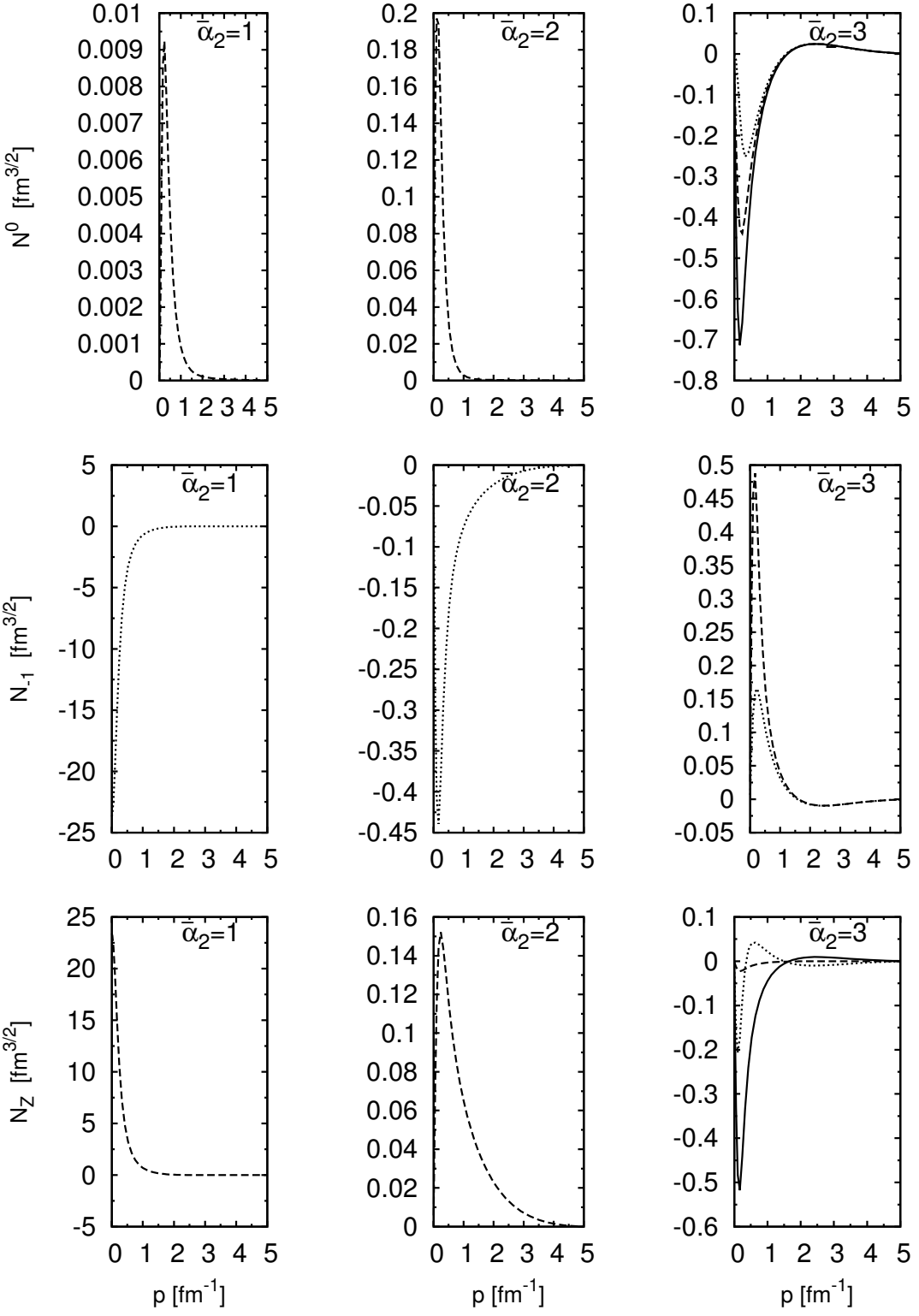

FIGURE 2.3: The nuclear matrix element $\langle p\bar{\alpha}_2 \mid j_w(1) \mid \phi_d \rangle$ for different partial wave states ($\bar{\alpha}_2 = 1, 2, 3$) at $E_\nu = 5$ MeV. In the three rows we show results for the weak density operator and two relevant components of the weak vector operator. The lines correspond to $m_d = -1$ (solid), $m_d = 0$ (dashed) and $m_d = 1$ (dotted). Note that for some (j, m_d) pairs these matrix elements are zero and thus not shown.

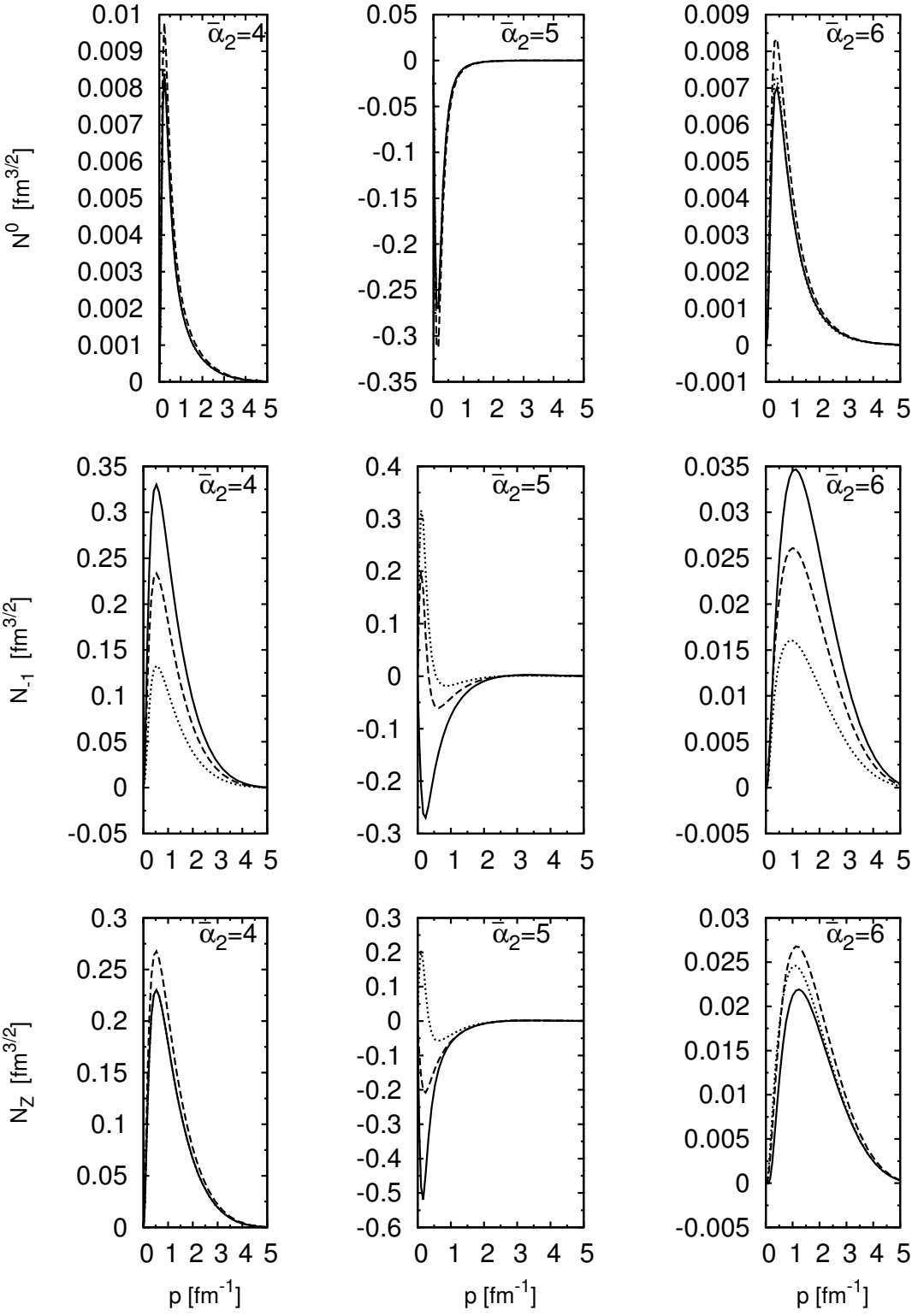

FIGURE 2.4: The same as in Fig. 2.3 but for $\bar{\alpha}_2 = 4, 5, 6$.

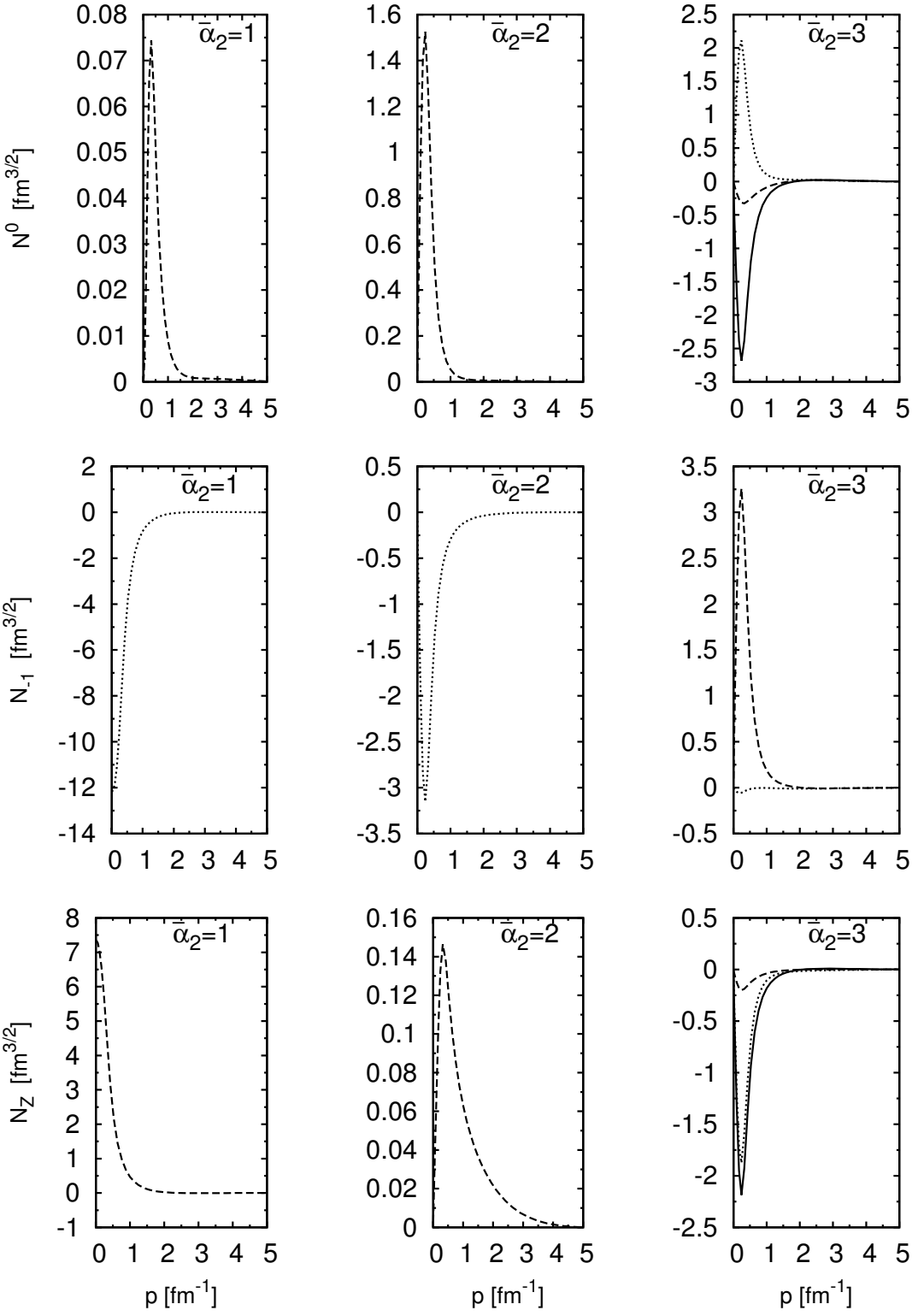

FIGURE 2.5: The same as in Fig. 2.3 but for $E_\nu = 95$ MeV.

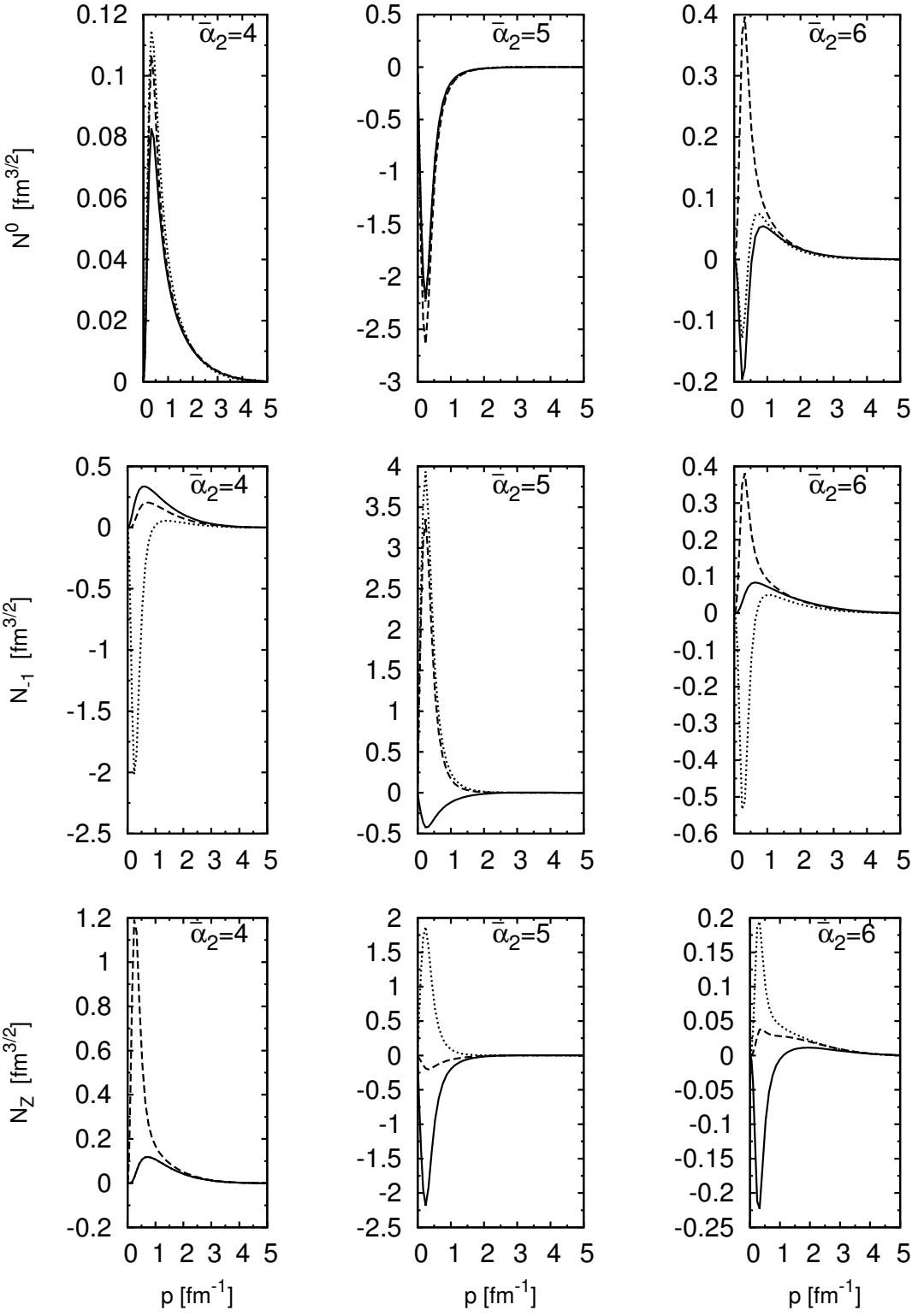

FIGURE 2.6: The same as in Fig. 2.5 but for $\bar{\alpha}_2 = 4, 5, 6$.

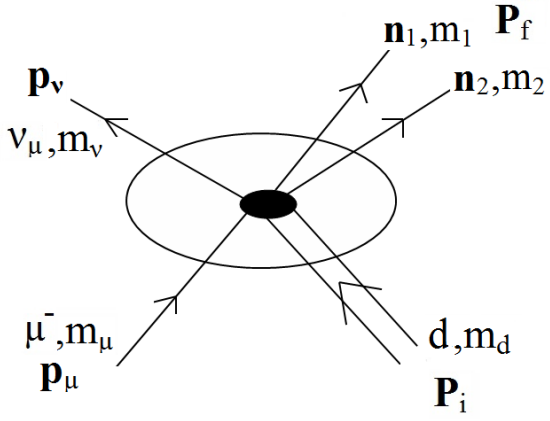

FIGURE 2.7: Diagram showing the very idea of the two-nucleon current operator. Both nucleons take part in the interaction with the lepton and the two-body mechanism is shown in the form of the filled oval.

currents are the "π-like and "ρ-like"currents:

$$\begin{aligned}\mathbf{j}^{(2)}_{ij}(\mathbf{k}_i,\mathbf{k}_j;\pi\mathrm{V}) &= \mathrm{i}\,(\tau_i\times\tau_j)_\pm\Big[v_{PS}(k_j)(\boldsymbol{\sigma}_i(\boldsymbol{\sigma}_j\cdot\mathbf{k}_j)-v_{PS}(k_i)\boldsymbol{\sigma}_j(\boldsymbol{\sigma}_i\cdot\mathbf{k}_i)\\ &\quad+\frac{\mathbf{k}_i-\mathbf{k}_j}{k_i^2-k_j^2}\big[v_{PS}(k_i)-v_{PS}(k_j)\big](\boldsymbol{\sigma}_i\cdot\mathbf{k}_i)(\boldsymbol{\sigma}_j\cdot\mathbf{k}_j)\Big]\ , \qquad (2.20)\end{aligned}$$

$$\begin{aligned}\mathbf{j}^{(2)}_{ij}(\mathbf{k}_i,\mathbf{k}_j;\rho\mathrm{V}) &= -\mathrm{i}\,(\tau_i\times\tau_j)_\pm\Big[v_V(k_j)\boldsymbol{\sigma}_i\times(\boldsymbol{\sigma}_j\times\mathbf{k}_j)-v_V(k_i)\boldsymbol{\sigma}_j\times(\boldsymbol{\sigma}_i\times\mathbf{k}_i)\\ &\quad-\frac{v_V(k_i)-v_V(k_j)}{k_i^2-k_j^2}\big[(\mathbf{k}_i-\mathbf{k}_j)(\boldsymbol{\sigma}_i\times\mathbf{k}_i)\cdot(\boldsymbol{\sigma}_j\times\mathbf{k}_j)\\ &\quad+(\boldsymbol{\sigma}_i\times\mathbf{k}_i)\,\boldsymbol{\sigma}_j\cdot(\mathbf{k}_i\times\mathbf{k}_j)+(\boldsymbol{\sigma}_j\times\mathbf{k}_j)\,\boldsymbol{\sigma}_i\cdot(\mathbf{k}_i\times\mathbf{k}_j)\big]\\ &\quad+\frac{\mathbf{k}_i-\mathbf{k}_j}{k_i^2-k_j^2}[v_{VS}(k_i)-v_{VS}(k_j)]\Big]\ , \qquad (2.21)\end{aligned}$$

where $\mathbf{k}_i$ and $\mathbf{k}_j$ are the momenta transferred to nucleons i and j with $\mathbf{Q}=\mathbf{k}_i+\mathbf{k}_j$. The isospin operators are defined as

$$(\tau_i\times\tau_j)_\pm\equiv(\tau_i\times\tau_j)_x\pm\mathrm{i}\,(\tau_i\times\tau_j)_y\ , \qquad (2.22)$$

and $v_{PS}(k)$, $v_V(k)$, and $v_{VS}(k)$ are given by

$$v_{PS}(k) = v^{\sigma\tau}(k)-2\,v^{t\tau}(k)\ , \qquad (2.23)$$

$$v_V(k) = v^{\sigma\tau}(k)+v^{t\tau}(k)\ , \qquad (2.24)$$

$$v_{VS}(k) = v^{\tau}(k)\ , \qquad (2.25)$$

with

$$v^{\tau}(k) = 4\pi \int_0^{\infty} r^2 dr\, j_0(kr) v^{\tau}(r) \ , \tag{2.26}$$

$$v^{\sigma\tau}(k) = \frac{4\pi}{k^2} \int_0^{\infty} r^2 dr\, \left[j_0(kr) - 1\right] v^{\sigma\tau}(r) \ , \tag{2.27}$$

$$v^{t\tau}(k) = \frac{4\pi}{k^2} \int_0^{\infty} r^2 dr\, j_2(kr) v^{t\tau}(r) \ . \tag{2.28}$$

Here $v^{\tau}(r)$, $v^{\sigma\tau}(r)$, $v^{t\tau}(r)$ are the isospin-dependent central, spin-spin, and tensor components of the AV18 two-nucleon interaction Other MI and all MD vector currents have been found numerically very small [11] compared with the "π-like"structures and we neglect them.

The "π-like"and "ρ-like"terms contribute also to the weak vector charge. They are in fact "model-dependent"but constitute numerically most important parts. They are given by:

$$\rho_{ij}^{(2)}(\mathbf{k}_i, \mathbf{k}_j; \pi\mathrm{V}) = -\frac{1}{M}\left[\tau_{j,\pm}\, v_{PS}(k_j)\, \boldsymbol{\sigma}_i \cdot \mathbf{Q}\, \boldsymbol{\sigma}_j \cdot \mathbf{k}_j + \tau_{i,\pm}\, v_{PS}(k_i)\, \boldsymbol{\sigma}_i \cdot \mathbf{k}_i\, \boldsymbol{\sigma}_j \cdot \mathbf{Q}\right] \ , \tag{2.29}$$

$$\rho_{ij}^{(2)}(\mathbf{k}_i, \mathbf{k}_j; \rho\mathrm{V}) = -\frac{1}{M}\Big[\tau_{j,\pm}\, v_V(k_j)(\boldsymbol{\sigma}_i \times \mathbf{Q}) \cdot (\boldsymbol{\sigma}_j \times \mathbf{k}_j) + \tau_{i,\pm}\, v_V(k_i)(\boldsymbol{\sigma}_j \times \mathbf{Q}) \cdot (\boldsymbol{\sigma}_i \times \mathbf{k}_i)\Big] \ , \tag{2.30}$$

where M is, as before, the average nucleon mass.

In contrast to the polar-vector case, the axial current operator is not conserved and its two-body components cannot be obtained from the nucleon-nucleon interaction. Thus they should be considered as model dependent. Following again [11] we list here only the axial current operators stemming from π- and ρ-meson exchanges:

$$\begin{aligned} \mathbf{j}_{ij}^{(2)}(\mathbf{k}_i, \mathbf{k}_j; \pi\mathrm{A}) \ = \ & - \ \frac{g_A}{2\,M}\, (\tau_i \times \tau_j)_{\pm}\, v_{PS}(k_j)\, \boldsymbol{\sigma}_i \times \mathbf{k}_j\, \boldsymbol{\sigma}_j \cdot \mathbf{k}_j \\ & + \ \frac{g_A}{M}\, \tau_{j,\pm}\, v_{PS}(k_j)\, (\mathbf{Q} + \mathrm{i}\, \boldsymbol{\sigma}_i \times \mathbf{P}_i)\, \boldsymbol{\sigma}_j \cdot \mathbf{k}_j + i \rightleftharpoons j \ , \end{aligned} \tag{2.31}$$

$$\begin{aligned} \mathbf{j}_{ij}^{(2)}(\mathbf{k}_i, \mathbf{k}_j; \rho\mathrm{A}) \ = \ & \frac{g_A}{2\,M}(\tau_i \times \tau_j)_{\pm}\, v_V(k_j) \Big[\mathbf{Q}\, \boldsymbol{\sigma}_i \cdot (\boldsymbol{\sigma}_j \times \mathbf{k}_j) + \mathrm{i}(\boldsymbol{\sigma}_j \times \mathbf{k}_j) \times \mathbf{P}_i \\ & - [\boldsymbol{\sigma}_i \times (\boldsymbol{\sigma}_j \times \mathbf{k}_j)] \times \mathbf{k}_j\Big] \\ & + \ \frac{g_A}{M}\tau_{j,\pm}\, v_V(k_j) \Big[(\boldsymbol{\sigma}_j \times \mathbf{k}_j) \times \mathbf{k}_j - \mathrm{i}[\boldsymbol{\sigma}_i \times (\boldsymbol{\sigma}_j \times \mathbf{k}_j)] \times \mathbf{P}_i\Big] \ + \ i \rightleftharpoons j \ , \end{aligned} \tag{2.32}$$

$$\mathbf{j}^{(2)}_{ij}(\mathbf{k}_i,\mathbf{k}_j;\rho\pi\mathrm{A}) = -\frac{g_A}{M}\,g_\rho^2\,(\tau_\mathbf{i}\times\tau_\mathbf{j})_\pm\,\frac{\mathbf{f}_\rho(\mathbf{k_i})}{\mathbf{k_i^2}+\mathbf{M_\rho^2}}\,\frac{\mathbf{f}_\pi(\mathbf{k_j})}{\mathbf{k_j^2}+\mathbf{M_\pi^2}}\,\boldsymbol{\sigma}_\mathbf{j}\cdot\mathbf{k_j} \times\Big[(1+\kappa_\rho)\,\boldsymbol{\sigma}_i\times\mathbf{k}_i-\mathrm{i}\mathbf{P}_i\Big]+i\rightleftharpoons j\ , \tag{2.33}$$

where $\mathbf{P}_i=\mathbf{p}_i+\mathbf{p}'_i$ is the sum of the initial ($\mathbf{p}_i$) and final ($\mathbf{p}'_i$) momenta of nucleon i. Note that we in this thesis use $v_{PS}(k)$ and $v_V(k)$ instead of $v_\pi(k)$ and $v_\rho(k)$ but this replacement has no significant impact on the calculations.

The last group of operators we deal with in this thesis constitute two-body weak axial charge operators. First we consider the so-called pion-range operator:

$$\rho^{(2)}_{ij}(\mathbf{k}_i,\mathbf{k}_j;\pi\mathrm{A}) = -\mathrm{i}\frac{g_A}{4\,\overline{f}_\pi^2}\,(\tau_i\times\tau_j)_\pm\,\frac{f_\pi^2(k_i)}{k_i^2+M_\pi^2}\,\boldsymbol{\sigma}_i\cdot\mathbf{k}_i+i\rightleftharpoons j\ , \tag{2.34}$$

where $\overline{f}_\pi$ is the pion decay constant ($\overline{f}_\pi\approx 93$ MeV) and $f_\pi(k)$ is the monopole form factor

$$f_\pi(k)=\frac{\Lambda_\pi^2-M_\pi^2}{\Lambda_\pi^2+k^2} \tag{2.35}$$

with $\Lambda_\pi=1.7$ GeV/c. Secondly, we include short-range axial charge operators associated with the central and spin-orbit components of the nucleon-nucleon interaction. The momentum-space expressions are taken again from [11] and read:

$$\rho^{(2)}_{ij}(\mathbf{k}_i,\mathbf{k}_j;\mathrm{sA}) = \frac{g_A}{2\,M^2}\,[\tau_{i,\pm}\,\overline{v}^{\,\mathrm{s}}(k_j)+\tau_{j,\pm}\,\overline{v}^{\,\mathrm{s}\tau}(k_j)]\,\boldsymbol{\sigma}_i\cdot\mathbf{P}_i+i\rightleftharpoons j\ , \tag{2.36}$$

$$\rho^{(2)}_{ij}(\mathbf{k}_i,\mathbf{k}_j;\mathrm{vA}) = \frac{g_A}{2\,M^2}\,[\tau_{i,\pm}\,\overline{v}^{\,\mathrm{v}}(k_j)+\tau_{j,\pm}\,\overline{v}^{\,\mathrm{v}\tau}(k_j)]\,[\boldsymbol{\sigma}_i\cdot\mathbf{P}_j+\mathrm{i}\,(\boldsymbol{\sigma}_i\times\boldsymbol{\sigma}_j)\cdot\mathbf{k}_j] -\mathrm{i}\,\frac{g_A}{4\,M^2}(\tau_i\times\tau_j)_\pm\,\overline{v}^{\,\mathrm{v}\tau}(k_j)\,\boldsymbol{\sigma}_i\cdot\mathbf{k}_i+i\rightleftharpoons j\ , \tag{2.37}$$

where

$$\overline{v}^{\,\alpha}(k)=4\pi\int_0^\infty dr\,r^2\,j_0(kr)\,\overline{v}^{\,\alpha}(r)\ , \tag{2.38}$$

with α=s, sτ, v, and vτ. The various scalar functions are defined in the following way:

$$\begin{aligned}\overline{v}^{\,\mathrm{s}}(r) &= \frac{3}{4}v^c(r)+\frac{m^2}{2}\int_r^\infty dr'\,r'\left[v^b(r')-\frac{1}{2}v^{bb}(r')\right]\\ \overline{v}^{\,\mathrm{v}}(r) &= \frac{1}{4}v^c(r)-\frac{M^2}{2}\int_r^\infty dr'\,r'\left[v^b(r')-\frac{1}{2}v^{bb}(r')\right]\ ,\end{aligned} \tag{2.39}$$

where $v^c(r)$, $v^b(r)$ and $v^{bb}(r)$ are the isospin-independent central, spin-orbit, and $(\mathbf{L}\cdot\mathbf{S})^2$ components of the AV18 potential. In order to obtain the definitions of $\overline{v}^{\,\mathrm{s}\tau}(r)$ and $\overline{v}^{\,\mathrm{v}\tau}(r)$, it is sufficient to replace in the above formulas the isospin-independent $v^c(r)$, $v^b(r)$ and $v^{bb}(r)$ with the isospin-dependent $v^{c\tau}(r)$, $v^{b\tau}(r)$ and $v^{bb\tau}(r)$.

Two-body contributions described in [11] contain also weak current and charge operators associated with excitations of the Δ isobars. They have been found to be most important numerically among all the two-body axial current operators. They are, however, given in such a form that they cannot be directly included in our momentum space framework. We decided to neglect them in this thesis and restrict ourselves to the two-body operators linked to meson exchanges.

We would like to stress that our way to include the rich set of two-nucleon operators is ready to deal with any expressions given in the momentum space. It was well tested in [28, 29], where many different two-nucleon current operators generated by the exchange of two pions, were incorporated in the description of electron induced deuteron break-up and deuteron photodisintegration reactions. We would like to remind the reader our basic formula for matrix elements of the current operator in our standard partial wave basis:

$$\begin{aligned}
&\langle p'(l's')j'm_{j'}\, t'm_{t'}\, \mathbf{P}_f \mid j_w(1,2) \mid p(ls)jm_j\, tm_t\, \mathbf{P}_i \rangle \;= \\
&\sum_{m_{l'}} \left(l', s', j'; m_{l'}, m_{j'} - m_{l'}, m_{j'}\right) \sum_{m_l} c\left(l, s, j; m_l, m_j - m_l, m_j\right) \\
&\int d\hat{\mathbf{p}}' \int d\hat{\mathbf{p}}\, Y^*_{l'\,m_{l'}}\left(\hat{\mathbf{p}}'\right)\, Y_{l\,m_l}\left(\hat{\mathbf{p}}\right) \\
&\left\langle s'm_{j'} - m_{l'};\, t'm_{t'} \mid \left\langle \mathbf{p}'\, \mathbf{P}_f \mid j_w^{\text{spin+isospin}}(1,2) \mid \mathbf{p}\, \mathbf{P}_i \right\rangle \mid sm_j - m_l;\, tm_t \right\rangle ,
\end{aligned} \tag{2.40}$$

where $\mathbf{p}$ ($\mathbf{p}'$) and $\mathbf{P}_i$ ($\mathbf{P}_f$) are the relative and total momenta of the two nucleons in the initial (final) state.

Using software for symbolic algebra, for example *Mathematica*® [21], we prepare momentum dependent spin-isospin matrix elements

$$\left\langle s'm_{j'} - m_{l'}\,;\, t'm_{t'} \mid \left\langle \mathbf{p}'\, \mathbf{P}_f \mid j_w^{\text{spin+isospin}}(1,2) \mid \mathbf{p}\, \mathbf{P}_i \right\rangle \mid sm_j - m_l\,;\, tm_t \right\rangle \tag{2.41}$$

separately for the total weak current and total weak charge operators in the reference frame where $\mathbf{Q} \equiv \mathbf{P}_f - \mathbf{P}_i \parallel \hat{\boldsymbol{z}}$. (Only such a choice yields a simple relation between the total angular momentum projections m_j and $m_{j'}$.) The numerical four fold integrations are performed on massively parallel computers of the Jülich Supercomputing Centre in Germany. To achieve fully converged results no more than 20 integral points are required in each of four dimensions.

Chapter 3

Muon capture on deuteron

In this chapter we present our results for the $\mu^- + {}^2\mathrm{H} \to \nu_\mu + n + n$ reaction. Although the steps leading from the general form of S_{fi} to the capture rates formula are standard, we give here formulas for kinematics and capture rates for all the studied reactions, expecting that they might become useful in future benchmark calculations.

3.1 Results for the $\mu^- + {}^2\mathrm{H} \to \nu_\mu + n + n$ reaction

The kinematics of this processes can be treated without any approximations both relativistically and nonrelativistically. We make sure that the non-relativistic approximation is fully justified by comparing values of various quantities calculated nonrelativistically and using relativistic equations. This is important, since our dynamics is entirely non-relativistic. In all cases the starting point is the energy and momentum conservation, where we neglect the very small binding energy of the muon atom and the neutrino mass, assuming that the initial deuteron and muon are at rest. In the case of the $\mu^- + {}^2\mathrm{H} \to \nu_\mu + n + n$ reaction it reads

$$\begin{aligned} M_\mu + M_d &= E_\nu + \sqrt{M_n^2 + \mathbf{p}_1{}^2} + \sqrt{M_n^2 + \mathbf{p}_2{}^2}\,, \\ \mathbf{p}_1 + \mathbf{p}_2 + \mathbf{p}_\nu &= 0 \end{aligned} \tag{3.1}$$

and the first equation in (3.1) is approximated nonrelativistically by

$$M_\mu + M_d = E_\nu + 2M_n + \frac{\mathbf{p}_1{}^2}{2M_n} + \frac{\mathbf{p}_2{}^2}{2M_n}\,. \tag{3.2}$$

The maximal relativistic and non-relativistic neutrino energies read correspondingly

$$(E_\nu^{max,nn})^{rel} = \frac{1}{2}\left(-\frac{4{M_n}^2}{M_d+M_\mu} + M_d + M_\mu\right) \tag{3.3}$$

and

$$(E_\nu^{max,nn})^{nrl} = 2\sqrt{M_d M_n + M_\mu M_n - {M_n}^2} - 2M_n\,. \tag{3.4}$$

Assuming $M_p = 938.272$ MeV, $M_n = 939.565$ MeV, $M_\mu = 105.658$ MeV, $M_d = M_p + M_n$ - 2.225 MeV, we obtain $(E_\nu^{max,nn})^{rel} = 99.5072$ MeV and $(E_\nu^{max,nn})^{nrl} = 99.5054$ MeV, respectively, with a difference which is clearly negligible.

Further we introduce the relative Jacobi momentum, $\mathbf{p} = \frac{1}{2}\,(\mathbf{p}_1 - \mathbf{p}_2\,)$, and write the energy conservation in a way which best corresponds to the nuclear matrix element calculations:

$$M_\mu + M_d = E_\nu + 2M_n + \frac{E_\nu^2}{4M_n} + \frac{\mathbf{p}^{\,2}}{M_n}\,. \tag{3.5}$$

In the nuclear matrix element, $\langle \Psi_f\,\mathbf{P}_f\,m_f \mid j_w^\lambda \mid \Psi_i\,\mathbf{P}_i\,m_i\,\rangle$, we deal with the deuteron in the initial state and with a two-neutron scattering state in the final state. Introducing the spin magnetic quantum numbers, we write

$$\begin{aligned}\langle \Psi_f\,\mathbf{P}_f\,m_f \mid j_w^\lambda \mid \Psi_i\,\mathbf{P}_i\,m_i\,\rangle &= {}^{(-)}\langle \mathbf{p}\;\mathbf{P}_f = -\mathbf{p}_\nu\,m_1\,m_2 \mid j_w^\lambda \mid \phi_d\,\mathbf{P}_i\,m_d\,\rangle \\ &= \langle \mathbf{p}\;\mathbf{P}_f = -\mathbf{p}_\nu\,m_1\,m_2 \mid \Big(1 + t(E_{nn})\,G_0^{nn}(E_{nn})\Big)\, j_w^\lambda \mid \phi_d\,\mathbf{P}_i\,m_d\,\rangle\,.\end{aligned} \tag{3.6}$$

Thus for a given nucleon-nucleon potential, V, the scattering state of two neutrons is generated by introducing the solution of the Lippmann-Schwinger equation, t:

$$t(E_{nn}) = V + t(E_{nn})\,G_0^{nn}(E_{nn})\,V\,, \tag{3.7}$$

where $G_0^{nn}(E_{nn})$ is the free 2N propagator and the relative energy in the two-neutron system is

$$E_{nn} = \frac{\mathbf{p}^{\,2}}{M_n} = M_\mu + M_d - E_\nu - 2M_n - \frac{E_\nu^2}{4M_n}\,. \tag{3.8}$$

We generate the deuteron wave function and solve Eq. (3.7) in momentum space. Note that here, as well as for the $A = 3$ systems, we use the average "nucleon mass" in the kinematics and in solving the Lippmann-Schwinger equation. The effect of this approximation on the $\mu^- + {}^2\mathrm{H} \to \nu_\mu + n + n$ reaction will be discussed below. Taking

all factors into account and evaluating the phase space factor in terms of the relative momentum, we arrive at the following expression for the total capture rate

$$\Gamma_d = \frac{1}{2} G^2 \frac{1}{(2\pi)^2} \frac{(M'_d \alpha)^3}{\pi} \int_0^{\pi} d\theta_{p_\nu} \sin\theta_{p_\nu} \int_0^{2\pi} d\phi_{p_\nu} \int_0^{E_\nu^{max,nn}} dE_\nu E_\nu^2 \frac{1}{2} M_n p$$
$$\int_0^{\pi} d\theta_p \sin\theta_p \int_0^{2\pi} d\phi_p \frac{1}{6} \sum_{m_d, m_\mu} \sum_{m_1, m_2, m_\nu} \left| L_\lambda(m_\nu, m_\mu) N^\lambda(m_1, m_2, m_d) \right|^2 , \quad (3.9)$$

where the factor $\frac{(M'_d \alpha)^3}{\pi}$ stems from the K-shell atomic wave function, $M'_d = \frac{M_d M_\mu}{M_d + M_\mu}$ and $\alpha \approx \frac{1}{137}$ is the fine structure constant. We can further simplify this expression, since for the unpolarized case the integrand does not depend on the neutrino direction and the azimuthal angle of the relative momentum, ϕ_p. Thus we set $\hat{\mathbf{p}}_\nu = -\hat{\mathbf{z}}$, choose $\phi_p = 0$ and introduce the explicit components of $N^\lambda(m_1, m_2, m_d)$, which yields

$$\Gamma_d = \frac{1}{2} G^2 \frac{1}{(2\pi)^2} \frac{(M'_d \alpha)^3}{\pi} 4\pi \int_0^{E_\nu^{max,nn}} dE_\nu E_\nu^2 \frac{1}{2} M p$$
$$2\pi \int_0^{\pi} d\theta_p \sin\theta_p \frac{1}{3} \sum_{m_d} \sum_{m_1, m_2} \Big(\left| N^0(m_1, m_2, m_d) \right|^2 + \left| N_z(m_1, m_2, m_d) \right|^2 +$$
$$2 \left| N_{-1}(m_1, m_2, m_d) \right|^2 + 2\mathrm{Re} \left(N^0(m_1, m_2, m_d) \left(N_z(m_1, m_2, m_d) \right)^* \right) \Big) . \quad (3.10)$$

This form is not appropriate when we want to calculate separately capture rates from two hyperfine states $F = \frac{1}{2}$ or $F = \frac{3}{2}$ of the muon-deuteron atom (see Fig. 3.1). In such a case we introduce the coupling between the deuteron and muon spin via standard Clebsch-Gordan coefficients $c(\frac{1}{2}, 1, F; m_\mu, m_d, m_F)$ and obtain

$$\Gamma_d^F = \frac{1}{2} G^2 \frac{1}{(2\pi)^2} \frac{(M'_d \alpha)^3}{\pi} 4\pi \int_0^{E_\nu^{max,nn}} dE_\nu E_\nu^2 \frac{1}{2} M p$$
$$2\pi \int_0^{\pi} d\theta_p \sin\theta_p \frac{1}{2F+1} \sum_{m_F} \sum_{m_1, m_2, m_\nu}$$
$$\Big| \sum_{m_\mu, m_d} c(\frac{1}{2}, 1, F; m_\mu, m_d, m_F) L_\lambda(m_\nu, m_\mu) N^\lambda(m_1, m_2, m_d) \Big|^2 . \quad (3.11)$$

For the sake of clarity, in Eqs. (3.9)–(3.11) we show the explicit dependence of N^λ on the spin magnetic quantum numbers.

From Eq. (3.11) one can easily read out the differential capture rate $d\Gamma_d^F / dE_\nu$. As shown

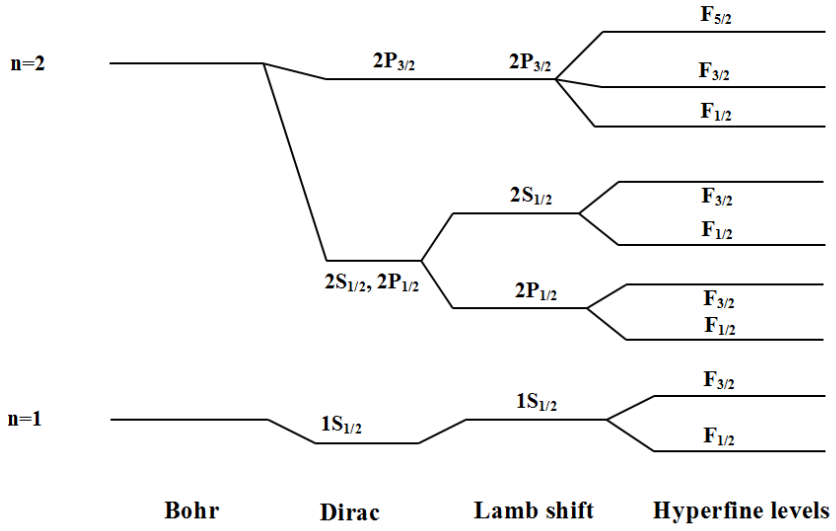

FIGURE 3.1: The splitting of the $n = 1$ and $n = 2$ levels of deuterium. The splittings are not to scale and are magnified from the left to the right of the diagram. The figure together with its caption is taken from Ref. [30]. It shows predictions of various theories for one-electron atoms: the non-relativistic Schrödinger equation, the Dirac equation, QED and including the hyperfine interactions.

in Fig. 3.2 this quantity soars in the vicinity of $E_\nu^{max,nn}$ (especially for the full results, that include the neutron-neutron final state interaction), what makes the observation of dynamical effects quite difficult. That is why the differential capture rate is usually shown as a function of the magnitude of the relative momentum. The transition between $d\Gamma_d^F/dE_\nu$ and $d\Gamma_d^F/dp$ is given by Eq. (3.8) and reads

$$\frac{d\Gamma_d^F}{dp} = \frac{d\Gamma_d^F}{dE_\nu}\left|\frac{dE_\nu}{dp}\right| = \frac{d\Gamma_d^F}{dE_\nu}\left|\frac{1}{\frac{dp}{dE_\nu}}\right| = \frac{4p}{E_\nu + 2M}\,\frac{d\Gamma_d^F}{dE_\nu}\,. \tag{3.12}$$

Our predictions shown in Figs. 3.2, 3.3 and 3.4 are obtained in the standard approach using partial wave decomposition (PWD), first for the Bonn B potential [31]. The calculations are performed including all partial wave states with $j \leq 4$. In some cases we include contributions from $j = 5$ and $j = 6$ states. We typically use 70 E_ν points and 50 θ_p values to achieve fully converged results.

These figures (and the corresponding numbers given in Table 3.1) show clearly that the doublet rate is dominant, as has been observed before, for example in Ref. [8]. Although the plane wave and full results for the total $F = \frac{1}{2}$ and $F = \frac{3}{2}$ rates are rather similar, the shapes of differential rates are quite different. The $1/M^2$ corrections in the current operator do not make significant contributions (see Fig. 3.4) and the total rate is reduced

only by about 2% for $F = \frac{1}{2}$ and raised by about 4% for $F = \frac{3}{2}$.

In Fig. 3.5 we see that our predictions calculated with different nucleon-nucleon potentials lie very close to each other. We take the older Bonn B potential [31], the AV18 potential [19] and five different parametrizations of the older chiral next-to-next-to-leading order (N2LO) potential from the Bochum-Bonn group [32]. The corresponding total $F = \frac{1}{2}$ rates vary only by about 2%, while the total $F = \frac{3}{2}$ rates are even more stable. It remains to be seen, if the same effects can be found with a more complicated current operator.

The doublet and quadruplet total capture rates are given in Table 3.1 with the various nucleon-nucleon potentials indicated above and the different approximations already discussed for Figs. 3.2-3.5. The experimental data of Refs. [33–36] are also shown. Since the experimental uncertainties for these data are very large, no conclusion can be drawn from a comparison with them. Thus the very precise data that are expected from the MuSun experiment [4] will be indeed vitally important.

In Ref. [14] we compare our results calculated in the momentum space with the predictions obtained in the coordinate-space framework of Ref. [8], by including the same single nucleon current operator and the same AV18 [19] nucleon-nucleon potential. For the calculations that employ the neutron mass (both in the Lippmann-Schwinger equation for the t-matrix and in the final state kinematics) and are performed with $j \leq 2$ partial wave states we obtain $\Gamma_d^{F=1/2} = 380$ s^{-1}, which should be compared with $\Gamma_d^{F=1/2} = 378$ s^{-1} from Ref. [8]. If we restrict ourselves only to the $^1S_0$ neutron-neutron partial wave, the numbers for $\Gamma_d^{F=1/2}$ read 237 s^{-1} and 235 s^{-1}, respectively. This proves a very good agreement with Ref. [8].

All the above results have been calculated using PWD. In the case of the Bonn B potential they have been compared with the predictions obtained employing the three-dimensional scheme from Ref. [37] and an excellent agreement has been found. Thus we believe that our calculations using the single nucleon current pass all the necessary tests and we can embark on the inclusion of the 2N contributions to the weak current operator described in Sec. 2.2 of Chapter 2. As already mentioned they are given in Ref. [11] for the AV18 nucleon-nucleon potential [19].

In Fig. 3.6 we show the differential capture rate $d\Gamma_d^F/dp$ for the $\mu^- + ^2\mathrm{H} \to \nu_\mu + n + n$ process, comparing the full results calculated using the single nucleon current operator with relativistic corrections to the predictions obtained with additional meson exchange currents [11]. The effects both for $F = \frac{1}{2}$ and $F = \frac{3}{2}$ are not big and we obtain only

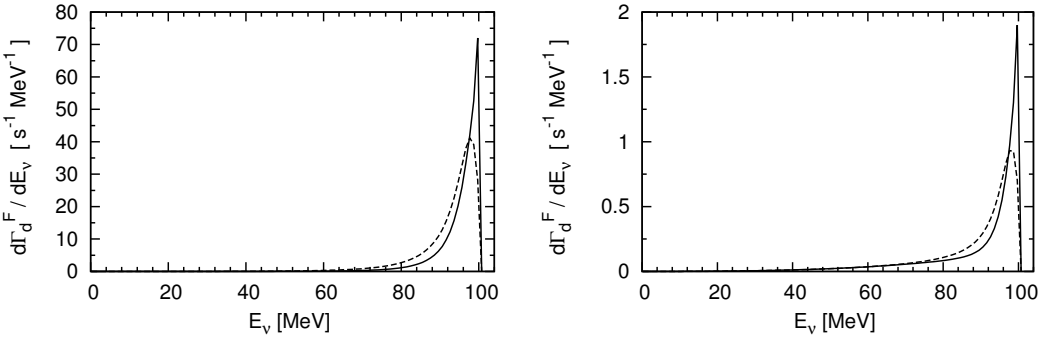

FIGURE 3.2: Differential capture rate $d\Gamma_d^F/dE_\nu$ for the $\mu^- + {}^2\mathrm{H} \to \nu_\mu + n + n$ process, calculated with the Bonn B potential [31] in the standard PWD approach, using the single nucleon current operator from Eqs. (2.7) and (2.8) for $F = \frac{1}{2}$ (left panel) and $F = \frac{3}{2}$ (right panel) as a function of the neutrino energy E_ν. The dashed curves show the plane wave results and the solid curves are used for the full results. Note that the average "nucleon mass" is used in the kinematics and in solving the Lippmann-Schwinger equations (see text for more details).

small shifts for the total capture rates:

$$\Gamma_d^{1/2}(\mathrm{PW}) : 361\ \mathrm{s}^{-1} \longrightarrow 367\ \mathrm{s}^{-1}$$
$$\Gamma_d^{1/2}(\mathrm{full}) : 392\ \mathrm{s}^{-1} \longrightarrow 401\ \mathrm{s}^{-1}$$
$$\Gamma_d^{3/2}(\mathrm{PW}) : 10.2\ \mathrm{s}^{-1} \longrightarrow 10.8\ \mathrm{s}^{-1}$$
$$\Gamma_d^{3/2}(\mathrm{full}) : 12.0\ \mathrm{s}^{-1} \longrightarrow 12.7\ \mathrm{s}^{-1}$$

In particular for the most important case of $\Gamma_d^{1/2}(\mathrm{full})$ the effect amounts to 2.3 %. (The corresponding result cannot be directly found in Ref. [8] but it has been confirmed by one of its authors [38].) For the electromagnetic reactions, especially for deuteron photodisintegration, meson-exchange currents are much more important, not only for the unpolarized cross sections but also for the polarization observables. To give the reader some idea about the scale of these effects, we show in Fig. 3.7 the total deuteron photodisintegration cross section as a function of the photon laboratory energy E_γ with the same AV18 potential [19] obtained within the framework described for example in [28]. Here the solid line represents the predictions obtained with additional "π-like"and "ρ-like"meson exchange currents closely corresponding to the vector currents from [11]. We see large effects that increase the single nucleon current predictions (dashed line) by more than a factor of 2.

In Ref. [8] further 2N operators are considered, which stem from the Δ excitations. Their contribution is far from being dominant but is visible for example in the ${}^1S_0$ partial wave. This type of operators is not included in this thesis.

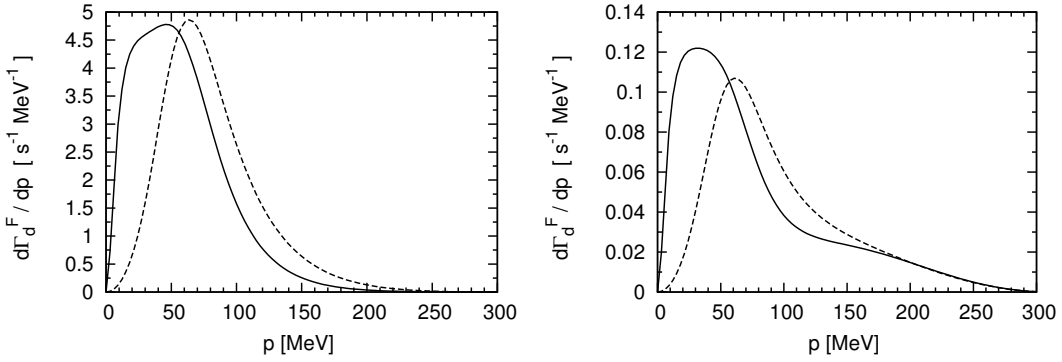

FIGURE 3.3: The same as in Fig. 3.2 but given in the form of $d\Gamma_d^F/dp$ and shown as a function of the magnitude of the relative neutron-neutron momentum p.

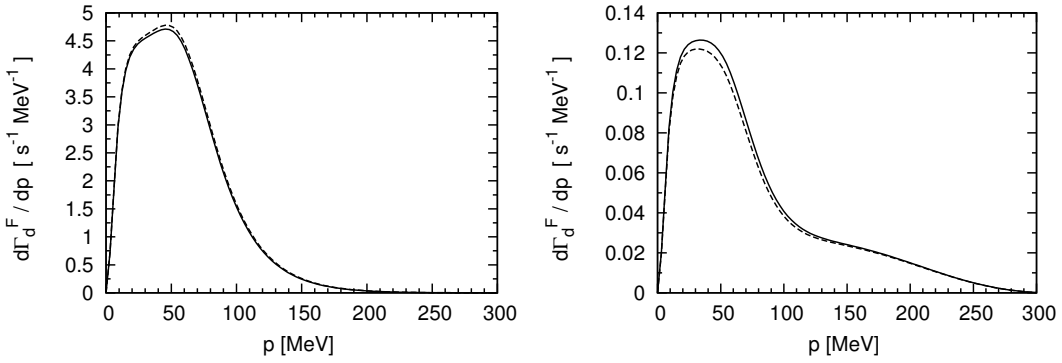

FIGURE 3.4: Differential capture rate $d\Gamma_d^F/dp$ of the $\mu^- + {}^2\mathrm{H} \to \nu_\mu + n + n$ process calculated with the Bonn B potential [31] for $F = \frac{1}{2}$ (left panel) and $F = \frac{3}{2}$ (right panel) as a function of the relative neutron-neutron momentum p. The dashed (solid) curves show the full results obtained with the single nucleon current operator without (with) the relativistic corrections. Note that the average "nucleon mass" is used in the kinematics and in solving the Lippmann-Schwinger equations (see text for more details).

Recently, the so-called "improved"chiral nucleon-nucleon potentials from the Bochum-Bonn group [18] were published. They are intended to replace the older chiral potentials [32] and due to the better regularization (performed in the coordinate space) are expected to yield a better description of nuclear structure and reactions. It is thus very exciting to obtain predictions based on this new nucleon-nucleon force, which is now available to us at different orders of the chiral expansion (from the lowest order up to even next-to-next-to-next-to-next-to leading order). This set of potentials is going to be widely used to solve the structure and reactions of light and heavier nuclei. So far no current operator consistent with this set of nucleon-nucleon potentials has been constructed, so the calculations are performed with the single nucleon current operator. In the thesis we present first results based on this new type of chiral forces for the $\mu^- + {}^2\mathrm{H} \to \nu_\mu + n + n$ reaction. In Table 3.2 we show results for the doublet and quadruplet capture rates calculated for all the available five orders of the chiral expansion and for all the five regulators at each order. We demonstrate also the spread of the full results for $F = 1/2$

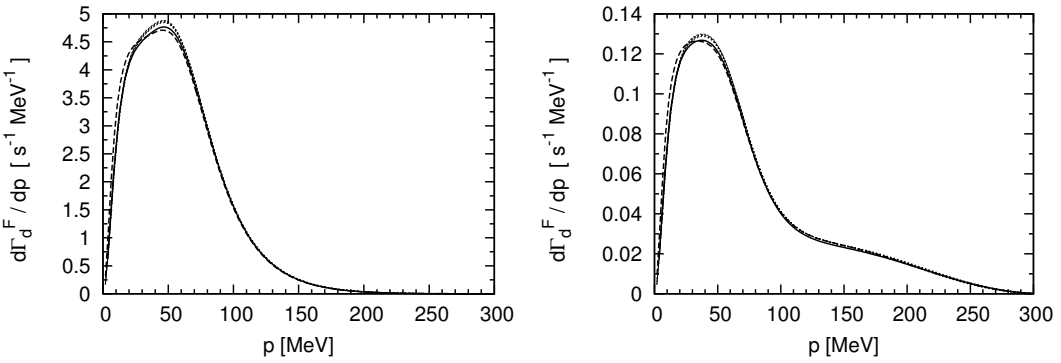

FIGURE 3.5: Differential capture rate $d\Gamma_d^F/dp$ of the $\mu^- + {}^2\mathrm{H} \to \nu_\mu + n + n$ process calculated using standard PWD with various nucleon-nucleon potentials: the AV18 potential [19] (solid curves), the Bonn B potential [31] (dashed curves) and the set of older chiral N2LO potentials from Ref. [32] (bands) for $F = \frac{1}{2}$ (left panel) and $F = \frac{3}{2}$ (right panel) as a function of the relative neutron-neutron momentum p. Note that the bands are very narrow and thus appear practically as a curve. All the partial wave states with $j \leq 4$ have been included in the calculations with the single nucleon current operator containing the relativistic corrections. Note that the average "nucleon mass" is used in the kinematics and in solving the Lippmann-Schwinger equations (see text for more details).

TABLE 3.1: Doublet ($F = 1/2$) and quadruplet ($F = 3/2$) capture rates for the $\mu^- + {}^2\mathrm{H} \to \nu_\mu + n + n$ reaction calculated with various nucleon-nucleon potentials and the single nucleon current operator without and with the relativistic corrections (RC). Plane wave results (PW) and results obtained with the rescattering term in the nuclear matrix element (full) are shown. Note that the average "nucleon mass" is used in the kinematics and in solving the Lippmann-Schwinger equations (see text for more details). The available experimental data are from Refs. [33–36].

	Capture rate Γ_d^F in s^{-1}			
	$F = 1/2$		$F = 3/2$	
nucleon-nucleon force and dynamics	PW	full	PW	full
Bonn B, without RC	369	403	10.0	11.7
Bonn B, with RC	363	396	10.4	12.2
AV18, with RC	361	392	10.2	12.0
chiral N2LO potential version 1 with RC	367	399	10.5	12.2
chiral N2LO potential version 2 with RC	364	394	10.4	12.2
chiral N2LO potential version 3 with RC	365	397	10.5	12.2
chiral N2LO potential version 4 with RC	367	399	10.4	12.2
chiral N2LO potential version 5 with RC	364	396	10.4	12.2
experimental results:				
I.-T. Wang *et al.* [33]	365 ± 96			
A. Bertin *et al.* [34]	445 ± 60			
G. Bardin *et al.* [35]	470 ± 29			
M. Cargnelli *et al.* [36]	409 ± 40			

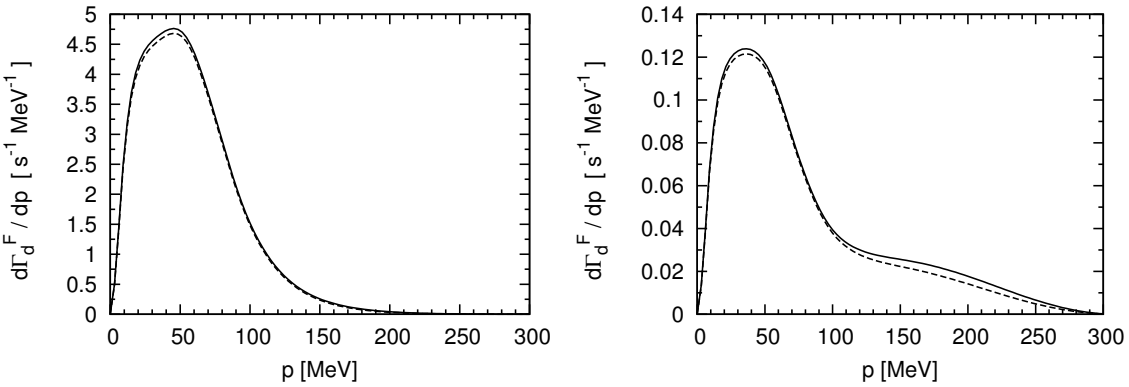

FIGURE 3.6: Differential capture rate $d\Gamma_d^F/dp$ for the $\mu^- + {}^2\mathrm{H} \to \nu_\mu + n + n$ process, calculated with the AV18 potential [19] for $F = \frac{1}{2}$ (left panel) and $F = \frac{3}{2}$ (right panel) as a function of the relative neutron-neutron momentum p. The dashed curves show the full results calculated using the single nucleon current operator with relativistic corrections. The solid lines represent the predictions obtained with additional meson exchange currents [11]. Now the proper neutron mass is used in the kinematics and in solving the Lippmann-Schwinger equations.

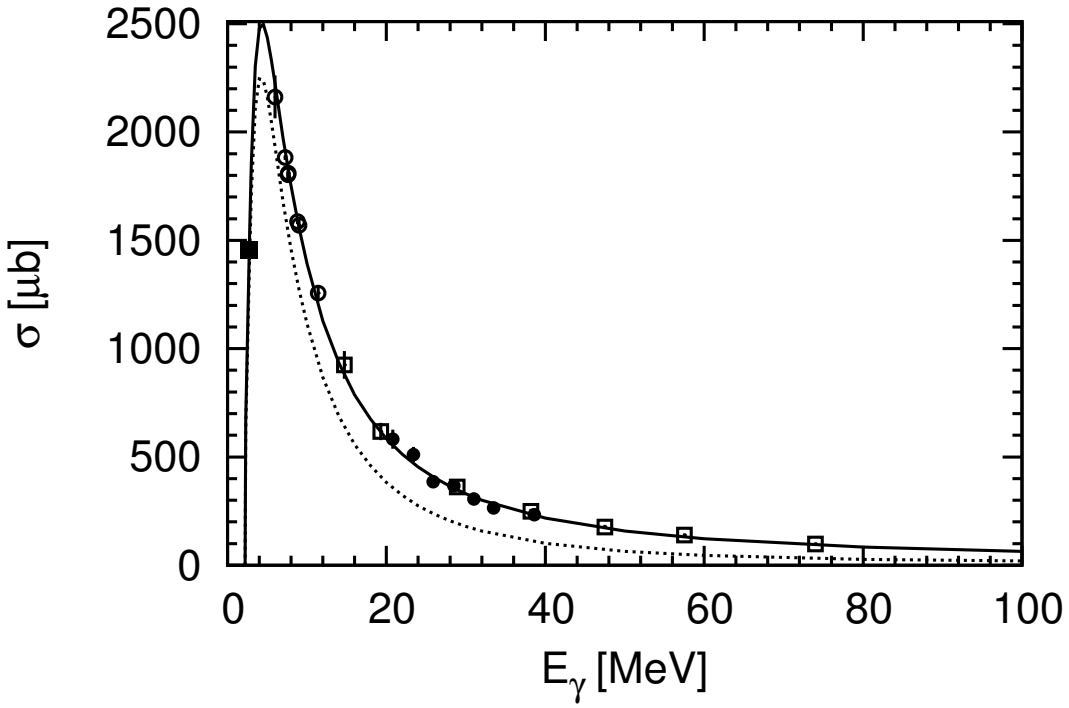

FIGURE 3.7: The total deuteron photodisintegration cross section σ as a function of the photon laboratory energy E_γ calculated in the center of mass frame with the AV18 potential [19]. The dashed curve shows the full results calculated using the single nucleon current operator. The solid line represents the predictions obtained with additional "π-like"and "ρ-like"meson exchange currents closely corresponding to the vector currents from [11]. Selected experimental data come from [39] (full circles), [40] (open circles), [41] (open squares), and [42] (full squares).

TABLE 3.2: Doublet ($F = 1/2$) and quadruplet ($F = 3/2$) capture rates for the $\mu^- + {}^2\mathrm{H} \to \nu_\mu + n + n$ reaction calculated with the improved chiral nucleon-nucleon potential [18] for different orders of the chiral expansion and the single nucleon current operator with the relativistic corrections (RC). Plane wave results (PW) and results obtained with the rescattering term in the nuclear matrix element (full) are shown. The neutron mass is used in the kinematics and in solving the Lippmann-Schwinger equations. All the partial waves with the total 2N angular momentum $j \leq 6$ are employed. In the last column the spread of the full results for $F = 1/2$ at the given order, $\Delta\Gamma_d^{1/2} \equiv \Gamma_{d\ max}^{1/2} - \Gamma_{d\ min}^{1/2}$, is also presented.

	Capture rate Γ_d^F in s^{-1}				
	$F = 1/2$		$F = 3/2$		
nucleon-nucleon force	PW	full	PW	full	$\Delta\Gamma_d^{1/2}$ in s^{-1}
LO with $R = 0.8$ fm	355.1	396.0	9.32	11.26	
LO with $R = 0.9$ fm	357.1	397.4	9.13	11.04	
LO with $R = 1.0$ fm	359.1	398.4	8.94	10.89	3.3
LO with $R = 1.1$ fm	361.1	398.9	8.78	10.59	
LO with $R = 1.2$ fm	362.9	399.2	8.63	10.38	
NLO with $R = 0.8$ fm	352.9	384.2	9.89	11.53	
NLO with $R = 0.9$ fm	353.8	385.8	9.88	11.53	
NLO with $R = 1.0$ fm	354.6	387.2	9.85	11.51	5.7
NLO with $R = 1.1$ fm	355.5	388.6	9.82	11.48	
NLO with $R = 1.2$ fm	356.3	389.8	9.77	11.45	
N2LO with $R = 0.8$ fm	354.2	385.0	9.83	11.60	
N2LO with $R = 0.9$ fm	354.9	386.1	9.84	11.56	
N2LO with $R = 1.0$ fm	355.5	387.2	9.84	11.53	4.3
N2LO with $R = 1.1$ fm	356.0	388.3	9.83	11.52	
N2LO with $R = 1.2$ fm	356.6	389.3	9.82	11.50	
N3LO with $R = 0.8$ fm	353.0	386.8	9.70	11.44	
N3LO with $R = 0.9$ fm	352.8	386.4	9.74	11.48	
N3LO with $R = 1.0$ fm	353.1	385.2	9.81	11.52	3.6
N3LO with $R = 1.1$ fm	353.8	384.3	9.91	11.58	
N3LO with $R = 1.2$ fm	354.5	383.2	10.05	11.66	
N4LO with $R = 0.8$ fm	353.1	385.5	9.77	11.51	
N4LO with $R = 0.9$ fm	354.0	386.1	9.78	11.50	
N4LO with $R = 1.0$ fm	354.8	386.3	9.81	11.50	1.7
N4LO with $R = 1.1$ fm	355.4	385.6	9.88	11.54	
N4LO with $R = 1.2$ fm	355.8	384.6	10.00	11.61	

at the given order, $\Delta\Gamma_d^{1/2} \equiv \Gamma_{d\ max}^{1/2} - \Gamma_{d\ min}^{1/2}$, due to various regulators used. Our results demonstrate a very welcome property of the new chiral forces, since the range of predictions obtained with different regulators gets narrower for the higher and higher orders of the chiral expansion. The spread of the results at N4LO is indeed very small and does not even reach 0.5 % !

We use one example of the improved chiral potential to study the convergence of our results with respect to the number of 2N partial waves. We see in Table 3.3 that the convergence is indeed very fast. The ${}^2\mathrm{H}(\mu^-, \nu\mu)nn$ muon-capture reaction is definitely

TABLE 3.3: Doublet ($F = 1/2$) and quadruplet ($F = 3/2$) capture rates for the $\mu^- + {}^2\mathrm{H} \to \nu_\mu + n + n$ reaction calculated with one example of the improved chiral nucleon-nucleon potential [18], using different numbers of two-nucleon basis states and the single nucleon current operator with the relativistic corrections (RC). The N4LO potential with the $R = 1$ fm regulator is used to generate plane wave results (PW) and results obtained with the rescattering term in the nuclear matrix elements (full). The neutron mass is used in the kinematics and in solving the Lippmann-Schwinger equations.

	Capture rate Γ_d^F in s^{-1}			
	$F = 1/2$		$F = 3/2$	
partial waves used	PW	full	PW	full
${}^1S_0$	210.0	240.5	4.84	6.38
$j_{max} \leq 1$	273.1	303.3	6.16	7.73
$j_{max} \leq 2$	351.9	383.4	9.62	11.31
$j_{max} \leq 3$	353.1	384.5	9.77	11.46
$j_{max} \leq 4$	354.7	386.2	9.81	11.50
$j_{max} \leq 5$	354.8	386.2	9.81	11.50
$j_{max} \leq 6$	354.8	386.3	9.81	11.50

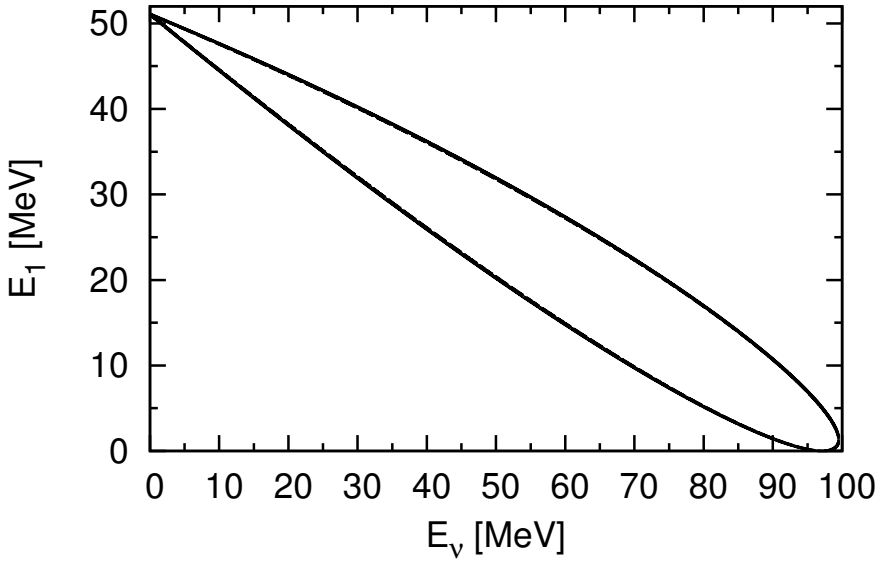

FIGURE 3.8: The kinematically allowed region in the $E_\nu - E_1$ plane calculated relativistically (solid line) and nonrelativistically (dashed line). The two line practically overlap.

a low energy phenomenon and can be successfully treated with a rather limited number of partial waves.

Our results given in the form of $d\Gamma_d^F/dE_\nu$ or $d\Gamma_d^F/dp$ cannot be compared *directly* with any experimental results. The muon neutrinos are very hard to detect and information about the two neutrons would be necessary to define the magnitude of the relative momentum. We ask ourselves a simple question: How to represent our results in the

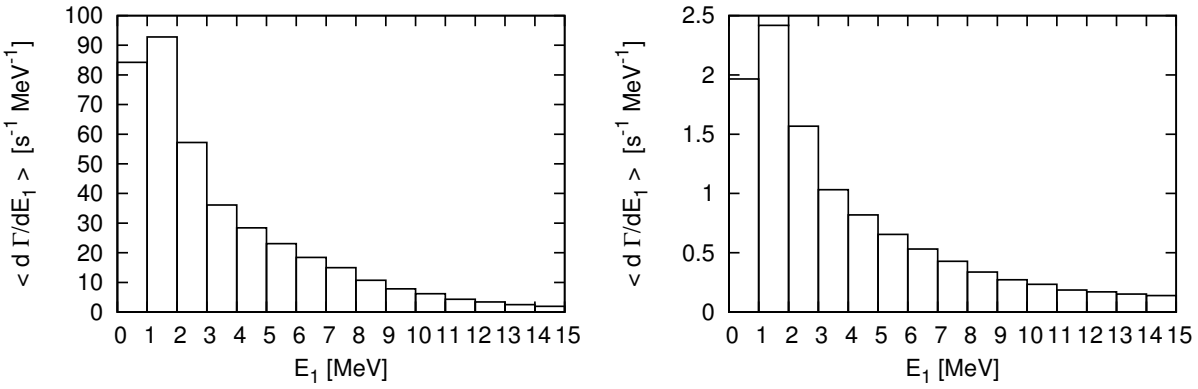

FIGURE 3.9: The doublet (left panel) and quadruplet (right panel) capture rates $\langle d\Gamma_d^F/dE_1\rangle$ for the $\mu^- + {}^2\mathrm{H} \to \nu_\mu + n + n$ reaction averaged over 1 MeV neutron energy bins calculated with the N4LO improved chiral nucleon-nucleon potential [18] with $R = 1$ fm regulator. The single nucleon current operator with the relativistic corrections (RC) is used.

form of the $d\Gamma_d^F/dE_1$, where E_1 is the kinetic energy of the outgoing neutron. (The kinematically allowed region in the $E_\nu - E_1$ plane is shown in Fig. 3.8.) We could in principle derive the expression for this differential capture rate but such a quantity cannot be measured in practice. So instead we consider the capture rates $\langle d\Gamma_d^F/dE_1\rangle$, which are averaged over certain neutron energy bins. They can be calculated, using just Eq. (3.11) but with an additional function $C(E_\nu, \theta_p)$ which evaluates to 1, if E_1 calculated from E_ν and θ_p lies within the $[E_1^{min}, E_1^{max}]$ interval or otherwise to zero.

$$\langle d\Gamma_d^F/dE_1\rangle = \frac{1}{2}G^2\frac{1}{(2\pi)^2}\frac{(M'_d\alpha)^3}{\pi}4\pi \int_0^{E_\nu^{max,nn}} dE_\nu E_\nu^2 \frac{1}{2}Mp$$
$$2\pi\int_0^\pi d\theta_p \sin\theta_p \frac{1}{2F+1}\sum_{m_F}\sum_{m_1,m_2,m_\nu}$$
$$\Big|\sum_{m_\mu,m_d} c(\frac{1}{2},1,F;m_\mu,m_d,m_F)\, L_\lambda(m_\nu,m_\mu) N^\lambda(m_1,m_2,m_d)\Big|^2$$
$$C(E_\nu,\theta_p)/\left(E_1^{max}-E_1^{min}\right) . \qquad (3.13)$$

In Figs. 3.9–3.11 we show these averaged capture rates first for 1 MeV and later for 5 MeV neutron energy bins. We employ the N4LO improved chiral nucleon-nucleon potential [18] with $R = 1$ fm regulator and the single nucleon current operator with the relativistic corrections. These calculations clearly show that the main contributions to the total capture rates come from the low-energy neutrons. This is bad news for the experiment, since such neutrons are difficult to detect.

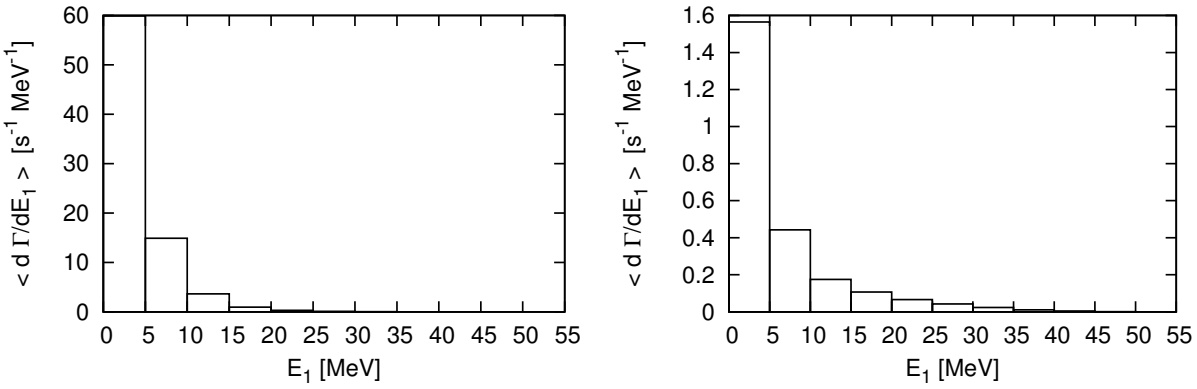

FIGURE 3.10: The same as in Fig. 3.9 for 5 MeV neutron energy bins.

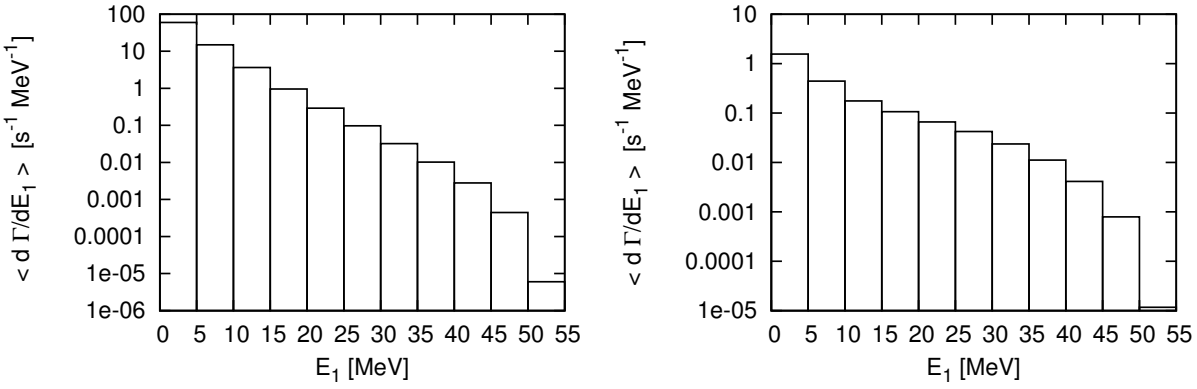

FIGURE 3.11: The same as in Fig. 3.10 but shown on the logarithmic scale.

Chapter 4

Muon capture reaction $^3\mathbf{He}(\mu^-, \nu_\mu)^3\mathbf{H}$

4.1 Results for the $\mu^- + ^3\mathrm{He} \rightarrow \nu_\mu + ^3\mathrm{H}$ reaction

In this case we deal with simple two-body kinematics and we can compare the neutrino energy calculated nonrelativistically and using relativistic equations. The relativistic result, based on

$$M_\mu + M_{^3\mathrm{He}} = E_\nu + \sqrt{E_\nu^2 + M_{^3\mathrm{H}}^2} \tag{4.1}$$

reads

$$(E_\nu)^{rel} = \frac{(M_{^3\mathrm{He}} + M_\mu)^2 - M_{^3\mathrm{H}}^2}{2\,(M_{^3\mathrm{He}} + M_\mu)}\,. \tag{4.2}$$

In the non-relativistic case, we start with

$$M_\mu + M_{^3\mathrm{He}} = E_\nu + M_{^3\mathrm{H}} + \frac{E_\nu^2}{2M_{^3\mathrm{H}}} \tag{4.3}$$

and arrive at

$$(E_\nu)^{nrl} = -M_{^3\mathrm{H}} + \sqrt{M_{^3\mathrm{H}}\,(-M_{^3\mathrm{H}} + 2\,(M_{^3\mathrm{He}} + M_\mu))}\,. \tag{4.4}$$

Again the obtained numerical values, $(E_\nu)^{rel} = 103.231$ MeV and $(E_\nu)^{nrl} = 103.230$ MeV, are very close to each other.

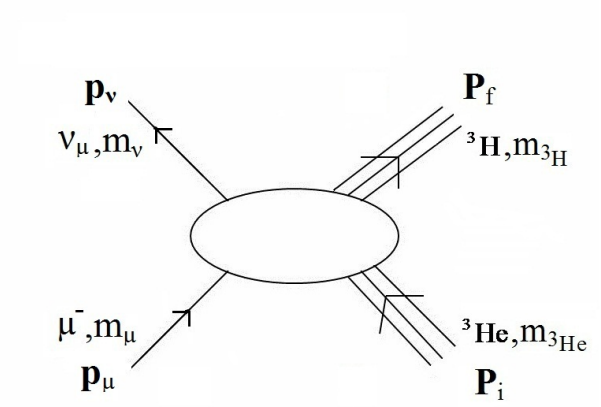

FIGURE 4.1: General diagram of the kinematics for the $\mu^- + ^3\mathrm{He} \to \nu_\mu + ^3\mathrm{H}$ reaction.

For this case we do not consider the ($F = 0$ and $F = 1$) hyperfine states in ^{3}He and calculate directly

$$\Gamma_{^3\mathrm{H}} = \frac{1}{2} G^2 \frac{1}{(2\pi)^2} \mathcal{R} \frac{\left(2M'_{^3\mathrm{He}}\alpha\right)^3}{\pi} \rho$$
$$4\pi \frac{1}{2} \sum_{m_{^3\mathrm{He}}} \sum_{m_{^3\mathrm{H}}} \Big(\left| N^0(m_{^3\mathrm{H}}, m_{^3\mathrm{He}}) \right|^2 + \left| N_z(m_{^3\mathrm{H}}, m_{^3\mathrm{He}}) \right|^2 +$$
$$2 \left| N_{-1}(m_{^3\mathrm{H}}, m_{^3\mathrm{He}}) \right|^2 + 2\mathrm{Re}\left(N^0(m_{^3\mathrm{H}}, m_{^3\mathrm{He}}) \left(N_z(m_{^3\mathrm{H}}, m_{^3\mathrm{He}})\right)^* \right) \Big), \quad (4.5)$$

where the factor $\frac{\left(2M'_{^3\mathrm{He}}\alpha\right)^3}{\pi}$, like in the deuteron case, comes from the K-shell atomic wave function and $M'_{^3\mathrm{He}} = \frac{M_{^3\mathrm{He}} M_\mu}{M_{^3\mathrm{He}} + M_\mu}$. Also in this case one can fix the direction of the neutrino momentum (our choice is $\hat{\mathbf{p}}_\nu = -\hat{\mathbf{z}}$) and the angular integration yields just 4π. The phase space factor ρ is

$$\rho = \frac{E_\nu^2}{1 + \frac{E_\nu}{\sqrt{E_\nu^2 + M_{^3\mathrm{H}}^2}}} \approx E_\nu^2 \left(1 - \frac{E_\nu}{M_{^3\mathrm{H}}}\right). \quad (4.6)$$

The additional factor $\mathcal{R}$ accounts for the finite volume of the ^{3}He charge and we adopt from [8] that $\mathcal{R} = 0.98$. (The corresponding factor in the deuteron case has been found to be very close to 1 [8] and thus is omitted.) Now, of course, the nuclear matrix elements involve the initial ^{3}He and final ^{3}H states:

$$N^\lambda(m_{^3\mathrm{H}}, m_{^3\mathrm{He}}) \equiv \langle \Psi_{^3\mathrm{H}}\, \mathbf{P}_f = -\mathbf{p}_\nu\, m_{^3\mathrm{H}} \mid j_w^\lambda \mid \Psi_{^3\mathrm{He}}\, \mathbf{P}_i = 0\, m_{^3\mathrm{He}} \rangle \quad (4.7)$$

and many-nucleon contributions are expected in j_w^λ as given in Eq. (2.19).

Our results for this process are given in Table 4.1. They are based on various 3N Hamiltonians necessary to generate the initial ^{3}He and final ^{3}H wave functions. These

wave functions were calculated by Dr. Andreas Nogga from the Jülich Research Center [43].

We use the single nucleon current operator. Only in the last line we show a result, where on top of the single nucleon contributions 2N operators are added to the current operator j_w^λ. We use the same meson-exchange currents from Ref. [11] as in Chapter 3, without Δ-isobar contributions. Our two last results from Table 4.1 (1324 s^{-1} and 1386 s^{-1}), should be compared with the PS (1316 s^{-1}) and Mesonic (1385 s^{-1}) predictions from Table X of Ref. [8], although not all the details of the calculations are the same. The experimental value for this capture rate is known with a rather good accuracy ($\Gamma_{exp} = (1496 \pm 4)$ s^{-1} [44]) so one can expect that the effects of 2N operators exceed 11%. At least for this process, they are more important than the 3N force effects. The latter ones amount roughly to 2% only. This dependence on the 3N interaction was already observed in Ref. [10], where it was shown that the total capture rate scales approximately linearly with the trinucleon binding energy.

Like in the 2N case, also in the 3N system we employ PWD and use our standard 3N basis $\mid pq\bar{\alpha}\, Jm_J; Tm_T \rangle$ [15], where p and q are magnitudes of the two relative Jacobi momenta and $\bar{\alpha}$ is a set of discrete quantum numbers. Note that the $\mid pq\bar{\alpha}\, Jm_J; Tm_T \rangle$ states are already antisymmetrized in the $(2,3)$ subsystem. Also in this case we have derived a general formula for PWD of the single nucleon current operator:

$$
\begin{aligned}
&\langle pq\bar{\alpha} Jm_J; Tm_T\, \mathbf{P}_f \mid j_w(1) \mid \Psi_{^3\mathrm{He}}\, \mathbf{P}_i = 0\, m_{^3\mathrm{He}}\, m_{T_b} \rangle = \\
&\sum_{\bar{\alpha}_b} \delta_{l,l_b}\, \delta_{s,s_b}\, \delta_{j,j_b}\, \delta_{t,t_b}\, \delta_{m_T,-\frac{1}{2}} \left\langle \left(t\tfrac{1}{2}\right) T\ -\tfrac{1}{2} \mid \tau_-(1) \mid \left(t_b\tfrac{1}{2}\right) \tfrac{1}{2}\,\tfrac{1}{2} \right\rangle \\
&\sum_{m_j} c\,(j, I, J; m_j, m_J - m_j, m_J)\ c\left(j_b, I_b, \frac{1}{2}; m_j, m_{^3\mathrm{He}} - m_j, m_{^3\mathrm{He}}\right) \\
&\sum_{m_\lambda} c\left(\lambda, \frac{1}{2}, I; m_\lambda, m_J - m_j - m_\lambda, m_J - m_j\right) \\
&\sum_{m_{\lambda_b}} c\left(\lambda_b, \frac{1}{2}, I_b; m_{\lambda_b}, m_{^3\mathrm{He}} - m_{j_b} - m_{\lambda_b}, m_{^3\mathrm{He}} - m_{j_b}\right) \\
&\int d\hat{\mathbf{q}}\, Y^*_{\lambda m_\lambda}(\hat{\mathbf{q}})\ Y_{\lambda_b m_{\lambda_b}}\left(\widehat{\mathbf{q} - \frac{2}{3}\mathbf{Q}}\right)\ \phi_{\bar{\alpha}_b}\left(p, \mid \mathbf{q} - \frac{2}{3}\mathbf{Q} \mid\right) \\
&\left\langle \frac{1}{2} m_J - m_j - m_\lambda \mid \left\langle \mathbf{q} + \frac{1}{3}\mathbf{P}_f \mid j_w^{\mathrm{spin}}(1) \mid \mathbf{q} - \frac{2}{3}\mathbf{P}_f + \mathbf{P}_i \right\rangle \mid \frac{1}{2} m_{^3\mathrm{He}} - m_{j_b} - m_{\lambda_b} \right\rangle
\end{aligned}
\tag{4.8}
$$

where, as in the 2N space, $\mathbf{Q} \equiv \mathbf{P}_f - \mathbf{P}_i$. We encounter again the essential spin matrix element

$$
\left\langle \frac{1}{2} m' \middle| \left\langle\, \mathbf{p}_1{}' \middle| j_w^{\mathrm{spin}}(1) \middle| \mathbf{p}_1 \,\right\rangle \middle| \frac{1}{2} m \right\rangle \tag{4.9}
$$

of the single nucleon current operator, which is calculated using software for symbolic algebra. The initial 3N bound state is given as

$$\mid \Psi_{^3\mathrm{He}}\, m_{^3\mathrm{He}} \rangle = \sum_{\bar{\alpha}_b} \int dpp^2 \int dqq^2 \left| pq\bar{\alpha}_b \, \frac{1}{2}\, m_{^3\mathrm{He}} \, ; \frac{1}{2}\frac{1}{2} \right\rangle \phi_{\bar{\alpha}_b}(p,q) \ . \tag{4.10}$$

In our calculations with these older Hamiltonians we use 34 (20) points for integration over p (q), and 34 partial wave states corresponding to $j \leq 4$.

In order to include the 2N contributions in the current operator in our PWD scheme, we have derived the following general formula:

$$\begin{aligned}
&\langle pq\bar{\alpha} J m_J; T m_T \, \mathbf{P}_f \mid j_w(2,3) \mid \Psi_{^3\mathrm{He}}\, \mathbf{P}_i \, m_{^3\mathrm{He}} \, m_{T_b} \rangle = \\
&\sum_{m_j} c\,(j,I,J; m_j, m_J - m_j, m_J\,) \sum_{\bar{\alpha}_b} \sum_{m_{j_b}} c\left(j_b, I_b, \frac{1}{2}; m_{j_b}, m_{^3\mathrm{He}} - m_{j_b}, m_{^3\mathrm{He}}\right) \\
&\sum_{m_l} c\,(l,s,j; m_l, m_j - m_l, m_j\,) \sum_{m_{l_b}} c\,(l_b, s_b, j_b; m_{l_b}, m_{j_b} - m_{l_b}, m_{j_b}\,) \\
&\sum_{m_t} c\left(t, \frac{1}{2}, T; m_t, m_T - m_t, m_T\right) \sum_{m_{t_b}} c\left(t_b, \frac{1}{2}, \frac{1}{2}; m_{t_b}, m_{T_b} - m_{t_b}, m_{T_b}\right) \\
&\sum_{m_\lambda} c\left(\lambda, \frac{1}{2}, I; m_\lambda, m_J - m_j - m_\lambda, m_J - m_j\right) \\
&\sum_{m_{\lambda_b}} c\left(\lambda_b, \frac{1}{2}, I_b; m_{\lambda_b}, m_{^3\mathrm{He}} - m_{j_b} - m_{\lambda_b}, m_{^3\mathrm{He}} - m_{j_b}\right) \\
&\left\langle \frac{1}{2} m_J - m_j - m_\lambda \mid m_{^3\mathrm{He}} - m_{j_b} - m_{\lambda_b} \right\rangle \int d\hat{\mathbf{p}} \int d\hat{\mathbf{q}} \int dp_b\, p_b^2 \int d\hat{\mathbf{p}}_b \\
&Y^*_{l,m_l}(\hat{\mathbf{p}})\; Y^*_{\lambda m_\lambda}(\hat{\mathbf{q}})\; Y_{l_b,m_{l_b}}(\hat{\mathbf{p}}_b)\; Y_{\lambda_b m_{\lambda_b}}\left(\widehat{\mathbf{q} + \frac{1}{3}\mathbf{Q}}\right) \phi_{\bar{\alpha}_b}\left(p_b, \mid \mathbf{q} + \frac{1}{3}\mathbf{Q} \mid\right) \\
&\left\langle s\, m_j - m_l \, ; \, t\, m_t \mid \left\langle \mathbf{p}\, \mathbf{q}\, \mathbf{P}_f \ \mid j_w^{\text{spin+isospin}}(2,3) \right.\right. \\
&\qquad\qquad \left.\left. \mid \mathbf{p}_b \ \mathbf{q} + \frac{1}{3}\mathbf{Q} \ \mathbf{P}_i \right\rangle \mid s_b\, m_{j_b} - m_{l_b} \, ; \, t_b\, m_{t_b} \right\rangle ,
\end{aligned} \tag{4.11}$$

where we use the notation: $\mathbf{p}_b = |\mathbf{p}_b|\,\hat{\mathbf{p}}_b \equiv p_b\,\hat{\mathbf{p}}_b$. The momentum dependence of the spin-isospin matrix elements,

$$\left\langle s\, m_s \, ; \, t\, m_t \mid \left\langle \mathbf{p}\, \mathbf{q}\, \mathbf{P}_f \ \mid j_w^{\text{spin+isospin}}(2,3) \mid \mathbf{p}_b\, \mathbf{q}_b\, \mathbf{P}_i \right\rangle \mid s_b\, m_{s_b} \, ; \, t_b\, m_{t_b} \right\rangle , \tag{4.12}$$

cannot be, in the general case, simplified and we deal with a substantial numerical task for some of the operators introduced in Sec. 2.2. Only for the so-called "local"operators, which depend on just two vector combinations, $\mathbf{p} - \mathbf{p}_b + \frac{1}{2}\mathbf{Q}$ and $-\mathbf{p} + \mathbf{p}_b + \frac{1}{2}\mathbf{Q}$, the angular integrals over $d\hat{\mathbf{p}}$ and $d\hat{\mathbf{p}}_b$ can be separated and prepared in advance, using essentially the same codes as for the 2N system. This is for example the case for the important "π-like and "ρ-like"electromagnetic current operators [15, 28, 29].

TABLE 4.1: Total capture rate Γ for the $\mu^- +^3$ He $\rightarrow \nu_\mu +^3$ H reaction calculated with the single nucleon current operator and various nucleon-nucleon potentials. In the last two lines the rates are obtained employing the AV18 [19] nucleon-nucleon and the Urbana IX 3N potential [20], and adding, in the last line, some selected 2Ns current operators to the single nucleon current (see text for more explanations).

Three-nucleon Hamiltonian	Capture rate Γ in s^{-1}
Bonn B	1360
chiral N2LO version 1	1379
chiral N2LO version 2	1312
chiral N2LO version 3	1350
chiral N2LO version 4	1394
chiral N2LO version 5	1332
AV18	1353
AV18 + Urbana IX	1324
AV18 + Urbana IX with MEC [11]	1386

We end this chapter by adding brand new results based on the improved chiral 2N forces [18], which ae given in Table 4.2. To the best of our knowledge, they are calculated for the first time. Like in the case of the $\mu^- +^2 \mathrm{H} \rightarrow \nu_\mu + n + n$ reaction, we demonstrate results for all the available orders of the chiral expansion and for all the five regulators at each order. Also for the $\mu^- +^3$ He $\rightarrow \nu_\mu +^3$ H reaction we calculate the spread of the results at the given order due to various regulators used. Starting from NLO, the range of predictions shrinks when we go to higher orders of the chiral expansion. The spread of the results at N4LO is, however, still significant ($\approx 1.8\%$) which might point to clear drawbacks of the calculations: the lack of consistent 3N forces and many-nucleon current operators. It will be very interesting to repeat these calculations with a complete dynamical framework.

TABLE 4.2: Total capture rate Γ for the $\mu^- + {}^3\mathrm{He} \to \nu_\mu + {}^3\mathrm{H}$ reaction calculated with the single nucleon current operator and the improved chiral nucleon-nucleon potentials from [18]. In the last column the spread of the predictions obtained for a given chiral order with different regulator parameters, $\Delta\Gamma \equiv \Gamma_{max} - \Gamma_{min}$, is also presented. In the last line we add, for the sake of comparison, the rate obtained employing the AV18 [19] nucleon-nucleon potential.

Nucleon-nucleon potential	Capture rate Γ in s^{-1}	$\Delta\Gamma$ in s^{-1}
LO with $R = 0.8$ fm	1610	
LO with $R = 0.9$ fm	1618	
LO with $R = 1.0$ fm	1610	46
LO with $R = 1.1$ fm	1594	
LO with $R = 1.2$ fm	1572	
NLO with $R = 0.8$ fm	1330	
NLO with $R = 0.9$ fm	1357	
NLO with $R = 1.0$ fm	1381	97
NLO with $R = 1.1$ fm	1405	
NLO with $R = 1.2$ fm	1427	
N2LO with $R = 0.8$ fm	1337	
N2LO with $R = 0.9$ fm	1356	
N2LO with $R = 1.0$ fm	1376	78
N2LO with $R = 1.1$ fm	1395	
N2LO with $R = 1.2$ fm	1415	
N3LO with $R = 0.8$ fm	1314	
N3LO with $R = 0.9$ fm	1304	
N3LO with $R = 1.0$ fm	1289	48
N3LO with $R = 1.1$ fm	1278	
N3LO with $R = 1.2$ fm	1266	
N4LO with $R = 0.8$ fm	1296	
N4LO with $R = 0.9$ fm	1307	
N4LO with $R = 1.0$ fm	1308	23
N4LO with $R = 1.1$ fm	1299	
N4LO with $R = 1.2$ fm	1285	
AV18	1353	

Chapter 5

Break-up channels in muon capture on ^{3}He

For the sake of completeness, we discuss here the formalism and some results for the two break-up reactions, $\mu^- + ^3\mathrm{He} \to \nu_\mu + n + d$ and $\mu^- + ^3\mathrm{He} \to \nu_\mu + n + n + p$. We stress, however, that our contribution to the presented results is restricted to the work on PWD of the single nucleon current operator. Thus this chapter is a short version of Sec. V from Ref. [14] and brings no new results compared to [14]. The results of this chapter have been obtained within the framework developed originally for electromagnetic reactions in the Cracow-Bochum group [15, 16].

5.1 Results for the $\mu^- + ^3\mathrm{He} \to \nu_\mu + n + d$ and $\mu^- + ^3\mathrm{He} \to \nu_\mu + n + n + p$ reactions

The kinematics of the $\mu^- + ^3\mathrm{He} \to \nu_\mu + n + d$ and $\mu^- + ^3\mathrm{He} \to \nu_\mu + n + n + p$ reactions is formulated in the same way as for the $\mu^- + ^2\mathrm{H} \to \nu_\mu + n + n$ process in Chapter. 3. The maximal neutrino energies for the two-body and three-body captures of the muon atom are evaluated as

$$\left(E_\nu^{max,nd}\right)^{rel} = \frac{(M_{^3\mathrm{He}} - M_d + M_\mu - M_n)(M_{^3\mathrm{He}} + M_d + M_\mu + M_n)}{2(M_{^3\mathrm{He}} + M_\mu)}\,, \tag{5.1}$$

$$(E_\nu^{max,nnp})^{rel} = \frac{{M_{^3\mathrm{He}}}^2 + 2M_{^3\mathrm{He}}M_\mu + {M_\mu}^2 - (2M_n + M_p)^2}{2(M_{^3\mathrm{He}} + M_\mu)}\,, \tag{5.2}$$

$$\left(E_\nu^{max,nd}\right)^{nrl} = \sqrt{(M_d + M_n)(2M_{^3\mathrm{He}} + 2M_\mu - M_d - M_n)} - M_d - M_n\,, \tag{5.3}$$

$$(E_\nu^{max,nnp})^{nrl} = \sqrt{(M_p + 2M_n)(2M_{^3\mathrm{He}} + 2M_\mu - 2M_n - M_p)} - 2M_n - M_p\,. \tag{5.4}$$

The numerical values are the following: $\left(E_\nu^{max,nd}\right)^{rel} = 97.1947$ MeV, $\left(E_\nu^{max,nd}\right)^{nrl} = 97.1942$ MeV, $(E_\nu^{max,nnp})^{rel} = 95.0443$ MeV and $(E_\nu^{max,nnp})^{nrl} = 95.0439$ MeV.

The kinematically allowed region in the $E_\nu - E_d$ plane for the two-body break-up of ^{3}He is shown in Fig. 5.1, calculated with the relativistic and nonrelativistic kinematics. They essentially overlap except for the very small neutrino energies. The same is also true for the three-body break-up as demonstrated in Fig. 5.2. Up to a certain E_ν value, which is denoted by E_ν^{2sol}, the minimal proton kinetic energy is zero. The minimal proton kinetic energy is greater than zero for $E_\nu > E_\nu^{2sol}$. Even this very detailed shape of the kinematical domain can be calculated nonrelativistically with high accuracy (see also the inset in Fig. 5.2). The values of E_ν^{2sol} based on the relativistic kinematics,

$$\left(E_\nu^{2sol}\right)^{rel} = \frac{(M_{^3\mathrm{He}} + M_\mu)(M_{^3\mathrm{He}} + M_\mu - 2M_p) - 4{M_n}^2 + {M_p}^2}{2(M_{^3\mathrm{He}} + M_\mu - M_p)} \tag{5.5}$$

and nonrelativistic kinematics,

$$\left(E_\nu^{2sol}\right)^{nrl} = 2\left(\sqrt{M_{^3\mathrm{He}}M_n + M_\mu M_n - {M_n}^2 - M_n M_p} - M_n\right)\,, \tag{5.6}$$

yield very similar numerical values, 94.2832 MeV and 94.2818 MeV, respectively.

The crucial matrix elements

$$N_{nd}^\lambda(m_n, m_d, m_{^3\mathrm{He}}) \equiv \langle \Psi_{nd}^{(-)}\, \mathbf{P}_f = -\mathbf{p}_\nu\, m_n\, m_d \mid j_w^\lambda \mid \Psi_{^3\mathrm{He}}\, \mathbf{P}_i = 0\, m_{^3\mathrm{He}} \rangle \tag{5.7}$$

and

$$N_{nnp}^\lambda(m_1, m_2, m_p, m_{^3\mathrm{He}}) \equiv \langle \Psi_{nnp}^{(-)}\, \mathbf{P}_f = -\mathbf{p}_\nu\, m_1\, m_2\, m_p \mid j_w^\lambda \mid \Psi_{^3\mathrm{He}}\, \mathbf{P}_i = 0\, m_{^3\mathrm{He}} \rangle \tag{5.8}$$

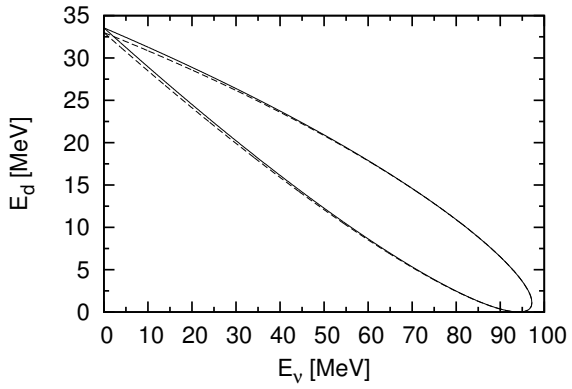

FIGURE 5.1: The kinematically allowed region in the $E_\nu - E_d$ plane calculated relativistically (solid curve) and nonrelativistically (dashed curve) for the $\mu^- + {}^3\mathrm{He} \to \nu_\mu + n + d$ process.

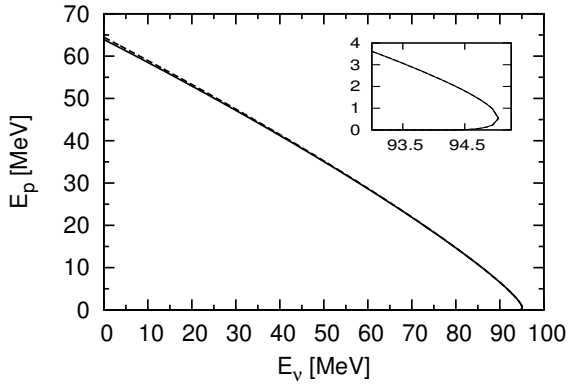

FIGURE 5.2: The kinematically allowed region in the $E_\nu - E_p$ plane calculated relativistically (solid curve) and nonrelativistically (dashed curve) for the $\mu^- + {}^3\mathrm{He} \to \nu_\mu + n + d$ process.

are calculated in two steps. First a Faddeev-like equation is solved for the auxiliary state $\mid U^\lambda \rangle$ for each considered neutrino energy:

$$\begin{aligned} \mid U^\lambda \rangle = \Big[tG_0 \, + \, \frac{1}{2}(1+P) V_4^{(1)} G_0 (1 + tG_0 \,) \Big] (1+P) j_w^\lambda \mid \Psi_{^3\mathrm{He}} \rangle \\ + \, \Big[tG_0 P \, + \, \frac{1}{2}(1+P) V_4^{(1)} G_0 (1 + tG_0 P \,) \Big] \mid U^\lambda \rangle \,, \end{aligned} \tag{5.9}$$

where $V_4^{(1)}$ is a part of the 3N force symmetrical under the exchange of nucleon 2 and 3, G_0 is the free 3N propagator and t is the 2N t-operator acting in the $(2,3)$ subspace. Further P is the permutation operator built from the transpositions P_{ij} exchanging nucleons i and j:

$$P = P_{12} P_{23} + P_{13} P_{23} \,. \tag{5.10}$$

In the second step the nuclear matrix elements are calculated by simple quadratures:

$$\begin{aligned} N^{\lambda}_{nd}(m_n, m_d, m_{^3\mathrm{He}}) &= \langle \phi_{nd}\, \mathbf{q}_0\, m_n\, m_d \mid (1+P) j^{\lambda}_w \mid \Psi_{^3\mathrm{He}} \rangle \\ &+ \langle \phi_{nd}\, \mathbf{q}_0\, m_n\, m_d \mid P \mid U^{\lambda} \rangle\,, \qquad (5.11) \\ N^{\lambda}_{nnp}(m_1, m_2, m_p, m_{^3\mathrm{He}}) &= \langle \phi_{nnp}\, \mathbf{p}\, \mathbf{q}\, m_1\, m_2\, m_p \mid (1+P) j^{\lambda}_w \mid \Psi_{^3\mathrm{He}} \rangle \\ &+ \langle \phi_{nnp}\, \mathbf{p}\, \mathbf{q}\, m_1\, m_2\, m_p \mid tG_0(1+P) j^{\lambda}_w \mid \Psi_{^3\mathrm{He}} \rangle \\ &+ \langle \phi_{nnp}\, \mathbf{p}\, \mathbf{q}\, m_1\, m_2\, m_p \mid P \mid U^{\lambda} \rangle \\ &+ \langle \phi_{nnp}\, \mathbf{p}\, \mathbf{q}\, m_1\, m_2\, m_p \mid tG_0 P \mid U^{\lambda} \rangle\,. \qquad (5.12) \end{aligned}$$

Here $\mid \phi_{nd}\, \mathbf{q}_0\, m_n\, m_d \rangle$ is a product state of the deuteron wave function and a momentum eigenstate of the spectator nucleon characterized by the relative momentum vector $\mathbf{q}_0$, while $\mid \phi_{nnp}\, \mathbf{p}\, \mathbf{q}\, m_1\, m_2\, m_p \rangle$ is a product state of two free motions in the 3N system given by Jacobi relative momenta $\mathbf{p}$ and $\mathbf{q}$, antisymmetrized in the $(2,3)$ subsystem. Equations (5.9), (5.11) and (5.12) simplify significantly, when $V_4^{(1)} = 0$ [16].

Finally we give the formulas for the total capture rates from [14]. Like for the $\mu^- + ^3\mathrm{He} \to \nu_\mu + ^3$ H reaction, also for the two break-up channels these quantities are calculated directly and the hyperfine states in ^{3}He are not considered. In the case of the two-body break-up it reads:

$$\begin{aligned} \Gamma_{nd} &= \frac{1}{2} G^2 \frac{1}{(2\pi)^2}\, \mathcal{R}\, \frac{\left(2M'_{^3\mathrm{He}}\alpha\right)^3}{\pi}\, 4\pi \\ &\int_0^{E_\nu^{max,nd}} dE_\nu E_\nu^2\, \frac{2}{3} M q_0\, \frac{1}{3} \int_0^{\pi} d\theta_{q_0} \sin\theta_{q_0}\, 2\pi \\ &\frac{1}{2} \sum_{m_{^3\mathrm{He}}} \sum_{m_n, m_d} \Big(\left| N^0_{nd}(m_n, m_d, m_{^3\mathrm{He}}) \right|^2 + \left| N_{nd,\,z}(m_n, m_d, m_{^3\mathrm{He}}) \right|^2 + \\ &2 \left| N_{nd,\,-1}(m_n, m_d, m_{^3\mathrm{He}}) \right|^2 + \\ &2\mathrm{Re}\left(N^0_{nd}(m_n, m_d, m_{^3\mathrm{He}})\, (N_{nd,\,z}(m_n, m_d, m_{^3\mathrm{He}}))^* \right) \Big)\,, \qquad (5.13) \end{aligned}$$

where the same arguments as before are used to simplify the angular integrations. The energy conservation is expressed in terms of the relative neutron-deuteron momentum

$$\mathbf{q}_0 \equiv \frac{2}{3} \left(\mathbf{p}_n - \frac{1}{2} \mathbf{p}_d \right)\,, \qquad (5.14)$$

yielding

$$M_\mu + M_{^3\mathrm{He}} \approx E_\nu + M_n + M_d + \frac{3}{4} \frac{\mathbf{q}_0^{\,2}}{M} + \frac{1}{6} \frac{E_\nu^2}{M}\,, \qquad (5.15)$$

where the deuteron binding energy is neglected. For the $\mu^- + {}^3\mathrm{He} \to \nu_\mu + n + n + p$ reaction the total capture rate Γ_{nnp} is obtained in a similar way:

$$\Gamma_{nnp} = \frac{1}{2} G^2 \frac{1}{(2\pi)^2} \mathcal{R} \frac{\left(2M'_{^3\mathrm{He}}\alpha\right)^3}{\pi} 4\pi$$
$$\int_0^{E_\nu^{max,nnp}} dE_\nu E_\nu^2 \frac{2}{3} M q \frac{1}{3} \int_0^\pi d\theta_q \sin\theta_q \, 2\pi \int_0^\pi d\theta_p \sin\theta_p \int_0^{2\pi} d\phi_p \int_0^{p^{max}} dp p^2$$
$$\frac{1}{2} \sum_{m_{^3\mathrm{He}}} \sum_{m_1,m_2,m_p} \Big(\left| N^0_{nnp}(m_1, m_2, m_p, m_{^3\mathrm{He}}) \right|^2 + \left| N_{nnp,\,z}(m_1, m_2, m_p, m_{^3\mathrm{He}}) \right|^2 +$$
$$2 \left| N_{nnp,\,-1}(m_1, m_2, m_p, m_{^3\mathrm{He}}) \right|^2 +$$
$$2\mathrm{Re}\left(N^0_{nnp}(m_1, m_2, m_p, m_{^3\mathrm{He}}) \left(N_{nnp,\,z}(m_1, m_2, m_p, m_{^3\mathrm{He}}) \right)^* \right) \Big) . \tag{5.16}$$

The energy conservation is expressed in terms of the Jacobi relative momenta $\mathbf{p}$ and $\mathbf{q}$

$$\mathbf{p} \equiv \frac{1}{2} \left(\mathbf{p}_1 - \mathbf{p}_2 \right) ,$$
$$\mathbf{q} \equiv \frac{2}{3} \left(\mathbf{p}_p - \frac{1}{2} \left(\mathbf{p}_1 + \mathbf{p}_2 \right) \right) , \tag{5.17}$$

which leads to

$$M_\mu + M_{^3\mathrm{He}} \approx E_\nu + 3M + \frac{\mathbf{p}^{\,2}}{M} + \frac{3}{4} \frac{\mathbf{q}^{\,2}}{M} + \frac{1}{6} \frac{E_\nu^2}{M} . \tag{5.18}$$

The discussion of predictions from [14] starts with Fig. 5.3, where for the $\mu^- + {}^3\mathrm{He} \to \nu_\mu + n + d$ reaction results of calculations employing all partial wave states are compared with the total subsystem angular momentum $j \leq 3$ and $j \leq 4$. Both the (symmetrized) plane wave and full results show a very good convergence and in practice it is sufficient to perform calculations with $j \leq 3$. We refer the reader to Ref. [15] for the detailed definitions of various 3N dynamics. A similar very rapid convergence is observed with respect to the total 3N angular momentum J. The differential capture rates $d\Gamma_{nd}/dE_{\nu_\mu}$ rise very slowly with the neutrino energy and show a strong maximum in the vicinity of the maximal neutrino energy. (At the very maximal neutrino energy the phase space factor reduces the differential rates to zero.) This maximum is broader for the plane wave case. Final state interaction effects are very important and in the maximum bring the full $d\Gamma_{nd}/dE_{\nu_\mu}$ to about 1/3 of the plane wave prediction. The results are based on the AV18 [19] nucleon-nucleon interaction.

In Fig. 5.4 results based on different 3N dynamics are displayed: plane wave approximation, symmetrized plane wave approximation, with the 3N Hamiltonian containing only 2N interactions and finally including also a 3N force (here the Urbana IX 3N potential [20]) both in the initial and final state. The effect of the 3N force on $d\Gamma_{nd}/dE_\nu$ is clearly

visible, since the maximum is reduced by about 20 %. From this figure one might draw the conclusion that the symmetrization in the plane wave matrix element is not important. This agreement between the plane wave and the symmetrized plane wave results is, however, rather accidental. As demonstrated in [14], the double differential capture rates $d^2\Gamma_{nd}/(dE_\nu d\Omega_{q_0})$ receive dominant contributions from different angular regions.

For the $\mu^- + {}^3\mathrm{He} \to \nu_\mu + n + n + p$ reaction (see Fig. 5.5) the convergence of the differential capture rate $d\Gamma_{nnp}/dE_\nu$ with respect to the number of partial wave states used in the full calculations is also very good. Comparing the shapes of $d\Gamma_{nd}/dE_\nu$ and $d\Gamma_{nnp}/dE_\nu$ it is clear that the latter becomes significantly different from zero at smaller neutrino energies. The calculations have been based in this case on the AV18 [19] nucleon-nucleon potential and 3N force effects have been neglected. Figure 5.6 shows 3N force effects adding the Urbana IX 3N force to the Hamiltonian. The peak reduction caused by the 3N force amounts to about 19 % which is quite similar to the two-body break-up case.

The results presented in Figs. 5.3–5.6 are supplemented by the corresponding values of integrated capture rates in Table 5.1, together with earlier theoretical predictions of Refs. [45–47] and experimental data from Refs. [48–51]. From inspection of the table one can conclude, first of all, that these results are fully at convergence. Secondly, one can estimate 3N force effects for the total rates. For the two break-up reactions separately (Γ_{nd} and Γ_{nnp}) as well as for the total break-up capture rate ($\Gamma_{nd} + \Gamma_{nnp}$) one deals with a reduction of their values by about 10 %, when the 3N force is included. Best predictions of [14] (obtained with the AV18 nucleon-nucleon potential and Urbana IX 3N force and the single nucleon current operator) are $\Gamma_{nd} = 544\ \mathrm{s}^{-1}$, $\Gamma_{nnp} = 154\ \mathrm{s}^{-1}$ and $\Gamma_{nd} + \Gamma_{nnp} = 698\ \mathrm{s}^{-1}$ and can be compared with the available experimental data gathered in Table 5.1, finding an overall nice agreement between theory and experiment for $\Gamma_{nd} + \Gamma_{nnp}$, except for the two results of Refs. [46, 47]. The experimental uncertainties are however quite large. When comparing with the latest experimental values of Ref. [51], one finds that the results from [18] for Γ_{nnp} are smaller than the experimental values and fall within the experimental estimates for Γ_{nd} and $\Gamma_{nd} + \Gamma_{nnp}$. One can expect that these predictions will be changed by about 10 %, when many body current operators are included in the framework.

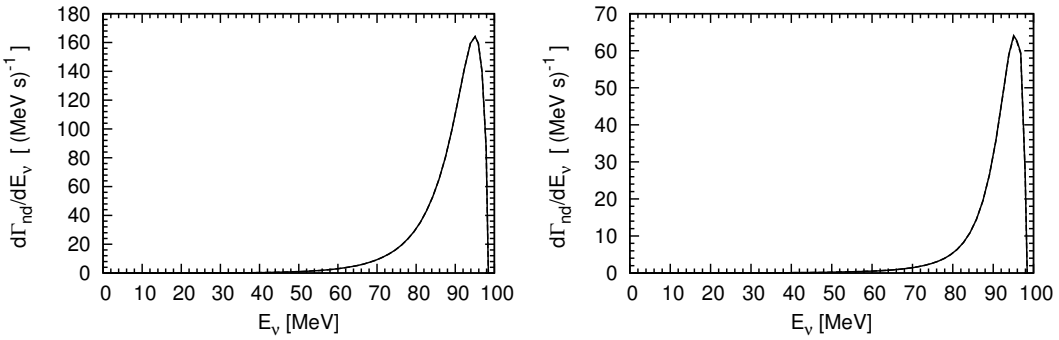

FIGURE 5.3: The differential capture rates $d\Gamma_{nd}/dE_\nu$ for the $\mu^- + ^3\text{He} \to \nu_\mu + n + d$ process calculated with the AV18 potential [19] and the single nucleon current operator as a function of the muon neutrino energy, using the symmetrized plane wave (left panel) and a full solution of Eq. (5.9) with $V_4^{(1)} = 0$ (right panel). The curves representing results of the calculations employing all partial wave states with $j \leq 3$ ($j \leq 4$) in the 2N subsystem are depicted with dashed (solid) curves. The maximal total 3N angular momentum is $J_{max} = \frac{9}{2}$.

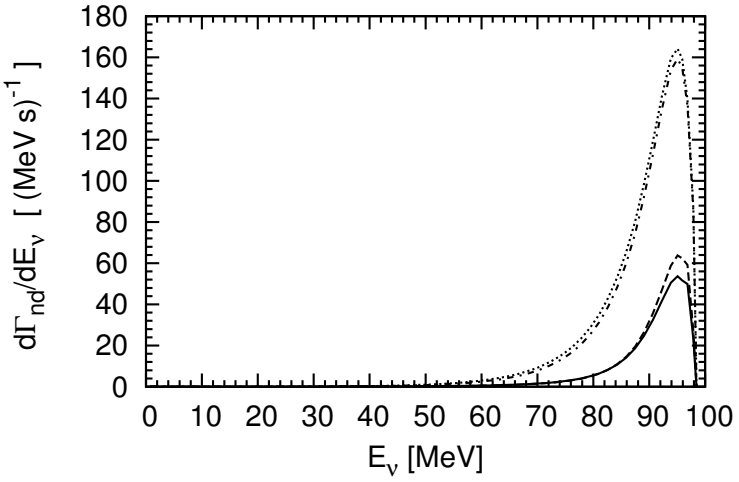

FIGURE 5.4: The differential capture rates $d\Gamma_{nd}/dE_\nu$ for the $\mu^- + ^3\text{He} \to \nu_\mu + n + d$ process calculated with the single nucleon current operator and different types of 3N dynamics: plane wave (dash-dotted curve), symmetrized plane wave (dotted curve), full solution of Eq. (5.9) without (dashed curve) and with 3N force (solid curve). The calculations are based on the AV18 nucleon-nucleon potential [19] and the Urbana IX 3N force [20] and employ all partial wave states with $j \leq 3$ and $J \leq \frac{9}{2}$.

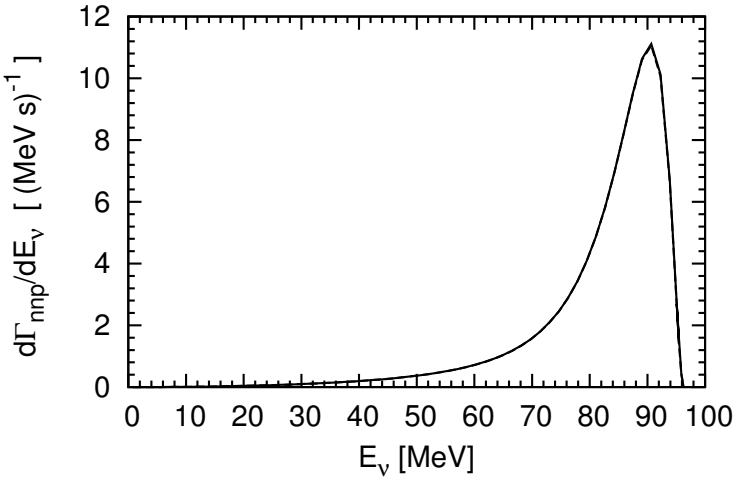

FIGURE 5.5: The differential capture rates $d\Gamma_{nnp}/dE_\nu$ for the $\mu^- + {}^3\mathrm{He} \to \nu_\mu + n + n + p$ process calculated with the AV18 potential [19] and using a full solution of Eq. (5.9) with $V_4^{(1)} = 0$. The curves representing results of the calculations employing all partial wave states with $j \leq 3$ ($j \leq 4$) in the 2N subsystem are depicted with dashed (solid) curves. The maximal total 3N angular momentum is $J_{max} = \frac{9}{2}$.

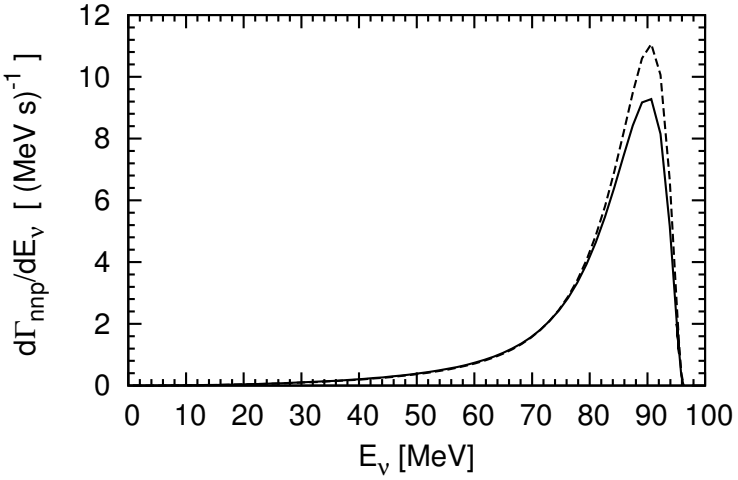

FIGURE 5.6: The differential capture rates $d\Gamma_{nnp}/dE_\nu$ for the $\mu^- + {}^3\mathrm{He} \to \nu_\mu + n + n + p$ process calculated with full solutions of Eq. (5.9) with $V_4^{(1)} = 0$ (dashed curve) and with $V_4^{(1)} \neq 0$ (solid curve). The calculations are based on the AV18 nucleon-nucleon potential [19] and the Urbana IX 3N force [20] and employ all partial wave states with $j \leq 3$ and $J \leq \frac{9}{2}$.

TABLE 5.1: Capture rates for the $\mu^- + ^3\text{He} \to \nu_\mu + n + d$ (Γ_{nd}) and $\mu^- + ^3\text{He} \to \nu_\mu + n + n + p$ (Γ_{nnp}) processes calculated with the AV18 [19] nucleon-nucleon potential and the Urbana IX [20] 3N force, using the single nucleon current and describing the final states just in plane wave (PW), symmetrized plane wave (SPW), and including final state interaction (full). Early theoretial predictions from Refs. [45–47] are also shown as well as experimental data are from Refs. [48–51].

	capture rate Γ in s^{-1}				
	Γ_{nd}			Γ_{nnp}	$\Gamma_{nd} + \Gamma_{nnp}$
	PW	SPW	full	full	full
AV18 ($j_{max} = 3$)	1917	2046	604	169	773
AV18 ($j_{max} = 4$)	1917	2046	606	170	776
AV18+Urbana IX ($j_{max} = 3$)	1853	1956	544	154	698
earlier theoretical predictions:					
A.F. Yano [45]		510		160	670
A.C. Philips *et al.* [46]		414		209	623
J.G. Congleton [47]					650
experimental results:					
O.A. Zaĭmidoroga *et al.* [48]					660 ± 160
L.B. Auerbach *et al.* [49]					$665\ ^{+170}_{-430}$
E.M. Maev *et al.* [50]					720 ± 70
V.M. Bystritsky *et al.* [51]:					
method I		491 ± 125		187 ± 11	678 ± 126
method II		497 ± 57		190 ± 7	687 ± 60

Chapter 6

Summary and conclusions

In Chapter 1 we try to describe the present-day status of few-nucleon studies concerning the muon-capture reactions on the lightest nuclei. It is clear that a consistent framework for the calculations of all muon capture processes on the deuteron, ^{3}He and other light nuclei should ultimately be prepared. This requires that the initial and final nuclear states are calculated with the same Hamiltonian and that the weak current operator is "compatible" with the nuclear forces. If results of such calculations can be compared with precise experimental data, our understanding of muon capture (and other) important weak reactions will be definitely improved.

In this thesis we report on substantial progress towards achieving this goal. The $\mu^- + {}^2\mathrm{H} \to \nu_\mu + n + n$, $\mu^- + {}^3\mathrm{He} \to \nu_\mu + {}^3\mathrm{H}$, $\mu^- + {}^3\mathrm{He} \to \nu_\mu + n + d$, and $\mu^- + {}^3\mathrm{He} \to \nu_\mu + n + n + p$ capture reactions are studied using a consistent momentum space framework with various realistic nucleon-nucleon potentials. We test our calculations in the case of the $\mu^- + {}^2\mathrm{H} \to \nu_\mu + n + n$ and $\mu^- + {}^3\mathrm{He} \to \nu_\mu + {}^3\mathrm{H}$ reactions, for which theoretical predictions obtained by the Pisa group with the same nuclear forces and current operators but using completely different methods are available. Calculations are now possible for the widely used realistic AV18 nucleon-nucleon potential [19] and two types of the weak current operator: the single nucleon one and the single nucleon current operator augmented by the meson-exchanged currents (partly at least) linked to the AV18 potential [11]. In the case of the $\mu^- + {}^2\mathrm{H} \to \nu_\mu + n + n$ we use results calculated within the scheme, which totally avoids standard partial wave decomposition [37] to cross-check further elements of our framework.

For each of the four reactions we start with a detailed analysis of the reaction kinematics. Exact results based on the relativistic and non-relativistic formulas are compared. In each case we find a beautiful agreement for both types of results, which gives us

confidence that also the non-relativistic dynamics we employ in our formalism is fully sufficient.

Chapter 2 introduces the detailed definitions of the weak current operator that is used in the thesis. Apart from the non-relativistic single nucleon current operator and the single nucleon current operator that contains relativistic corrections, we adopt meson exchange currents from Ref. [11]. What is even more important we introduce general formulas for the partial wave representation of these currents and describe a very efficient way to obtain the necessary PWD matrix elements. It utilizes software for symbolic algebra, for example *Mathematica*® [21], to prepare momentum dependent spin matrix elements.

In Chapter 3 we demonstrate our results for the $\mu^- + {}^2\mathrm{H} \to \nu_\mu + n + n$ capture process. We show predictions for the differential and total capture rates calculated with quite many different nucleon-nucleon potentials and the single nucleon current operator. We supplement information given in the literature by yielding predictions for the quadruplet differential and total capture rates. As already mentioned, our results calculated with the AV18 potential and the corresponding meson-exchange currents confirm earlier findings of the Pisa group in a completely independent way. We study different forms of the differential capture rates and show the phase-space regions with maximal contributions to the total rate.

Last not least, we show for the first time results based on the new, improved chiral potentials from the Bochum-Bonn group [18]. These new nucleon-nucleon forces are available for five orders of the chiral expansion and (at each order) with five different regularizations. Our results demonstrate a very welcome property of the new chiral forces since the range of predictions obtained at a given order but for five different regulators becomes very narrow when going to higher and higher orders of the chiral expansion. The spread of the results at N4LO is below 0.5 % !

In Chapter 4 we focus on the $\mu^- + {}^3\mathrm{He} \to \nu_\mu + {}^3\mathrm{H}$ capture reaction. For this two-body reaction we show predictions for the total rate, based again on various nucleon-nucleon potentials and the single nucleon current operator. Like in the previous chapter, we use a very safe method for PWD, now in the three-nucleon system. Since the 2N currents from [11] are "non-local"we have to generalize our method for PWD of 2N operators introduced in [15, 28]. The best result based on the AV18 nucleon-nucleon potential [19], the Urbana IX three-nucleon potential [20] and the current operator including meson-exchange contributions from [11] agrees very well with the one given in [8]. We would like to emphasize that all the three-nucleon bound states have been generated by Dr. Andreas Nogga [43].

Also for this reaction, we show for the first time results based on the new, improved chiral potentials from the Bochum-Bonn goup [18]. The predictions have the same tendency as for the $\mu^- + {}^2\mathrm{H} \to \nu_\mu + n + n$ case.

For the sake of completeness of our discussion we adopt in Chapter 5 the formalism and selected results for the two break-up reactions, $\mu^- + {}^3\mathrm{He} \to \nu_\mu + n + d$ and $\mu^- + {}^3\mathrm{He} \to \nu_\mu + n + n + p$. The results of this chapter have been obtained within the framework developed originally for electromagnetic reactions in the Cracow-Bochum group [15, 16] using the single nucleon current operator and older nuclear forces. We repeat, however, that our contribution to the presented results is restricted to the work on PWD of the single nucleon current operator. That chapter is a short version of Sec. V from Ref. [14] and brings no new results compared to [14].

The thesis contains additionally four appendices. Appendix A and Appendix B show two simple warm-up exercises, where we obtain numerically the muon and neutron lifetimes. We cross-check in this way our *Mathematica*® [21] tools, which are later used to calculate momentum dependent spin-isospin matrix elements in Chapters 2, 3 and 4. Appendix C deals with the numerical calculation of the deuteron wave function in the partial wave basis of the momentum space. Appendix D shows how to obtain the numerical solution of the Lippmann-Schwinger equation.

We strongly believe that the presented predictions will serve as an important benchmark for the future. We do hope that in the near future all the muon capture processes described in the thesis will be studied with the inclusion of at least 2N contributions to the nuclear current operators consistent with the nuclear forces. We definitely plan to use our framework also for neutrino-induced reactions on the deuteron and ^{3}He.

Appendix A

Muon decay

The muon decay process,

$$\mu^- \to \nu_\mu + e^- + \bar{\nu}_e \,,$$

is definitely worth studying because in the relevant matrix element one encounters exactly the same muonic part which appears in muon capture on light nuclei. On the other hand, the electronic part is the same as in the neutron beta decay reaction. This purely leptonic decay involves only elementary particles.

We decided to repeat the exercise of calculating the muon lifetime because one can learn how to treat the kinematics of three-particle decays. Additionally, we can test our *Mathematica*® [21] notebooks and, using them, significantly simplify the calculations. In particular, we do not use any trace identities. As the starting point to calculate the total muon decay rate (the inverse of the muon lifetime) we take directly Eqs. (2.18)

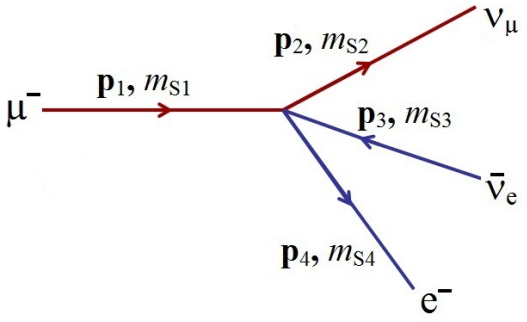

FIGURE A.1: muon decay diagram where $\mathbf{p}_i$, m_{s_i} is the three-momentum vector and the spin projection respectively.

and (2.19a) from [52] and apply it to the muon rest frame:

$$W = \frac{G^2}{2}\,\frac{1}{(2\pi)^5}\,\frac{1}{2m_1}\int\frac{d^3p_2}{2E_2}\int\frac{d^3p_3}{2E_3}\int\frac{d^3p_4}{2E_4}$$
$$\delta^4\left(\tilde{p}_2+\tilde{p}_3+\tilde{p}_4-\tilde{p}_1\right)\frac{1}{2}\sum_{m_{s_1},m_{s_2},m_{s_3},m_{s_4}}\mid\mathcal{M}\mid^2\,. \tag{A.1}$$

where we encounter the four-momenta of the initial muon at rest ($\tilde{p}_1=(m_1,\mathbf{p}_1=0)$) and outgoing particles: the massless muon neutrino ($\tilde{p}_2=(E_2=\mid\mathbf{p}_2\mid,\mathbf{p}_2)$), the massless electron antineutrino ($\tilde{p}_3=(E_3=\mid\mathbf{p}_3\mid,\mathbf{p}_3)$), and the electron ($\tilde{p}_4=(E_4,\mathbf{p}_4)$). The essential quantity $\mathcal{M}$ is given as a contraction of the muonic and electronic parts [52]

$$\mathcal{M}=\Big(\bar{u}(\mathbf{p}_2,m_{s_2})\gamma^\lambda(1-\gamma_5)u(\mathbf{p}_1,m_{s_1})\Big)\Big(\bar{u}(\mathbf{p}_4,m_{s_4})\gamma_\lambda(1-\gamma_5)v(\mathbf{p}_3,m_{s_3})\Big)\,, \tag{A.2}$$

where no additional parameter appears. Note that in this appendix we use the spinor normalization of Ref. [52].

In Eq. (A.1) we average over the initial muon spin projections and sum over spin projections of the outgoing particles, so

$$\mathcal{R}\equiv\frac{1}{2}\sum_{m_{s_1},m_{s_2},m_{s_3},m_{s_4}}\mid\mathcal{M}\mid^2$$

depends only on dot products of the momentum vectors of the three outgoing particles. With the help of *Mathematica*® [21] we arrive at:

$$\mathcal{R}=128\,m_1\mid\mathbf{p}_3\mid\Big(E_4\mid\mathbf{p}_2\mid-\mathbf{p}_2\cdot\mathbf{p}_4\Big)\,. \tag{A.3}$$

Having obtained this general result for $\mathcal{R}$ in (A.3), we can now decide how to calculate the integrals in Eq. (A.1). Because of the scalar nature of $\mathcal{R}$ and due to the four-momentum conservation, we are left with two dimensional integrals.

For the same reasons as in Section B we are left with a two dimensional integral. We choose:

$$\begin{aligned}\mathbf{p}_1&=(0,0,0)\,,\\ \mathbf{p}_4&=(0,0,\mid\mathbf{p}_4\mid)\,,\qquad\mid\mathbf{p}_4\mid\in[0,\mid\mathbf{p}_4\mid^{max}]\,,\\ \mathbf{p}_2&=(\mid\mathbf{p}_2\mid\sin\theta_{24},0,\mid\mathbf{p}_2\mid\cos\theta_{24})\,,\mathbf{p}_3=-\mathbf{p}_2-\mathbf{p}_4\,,\end{aligned} \tag{A.4}$$

where for massless neutrinos

$$\mid\mathbf{p}_4\mid^{max}=\sqrt{\frac{\left(m_1^2+m_4^2\right)^2}{4m_1^2}-m_4^2} \tag{A.5}$$

and the magnitude of the electron antineutrino momentum is calculated as

$$\mid \mathbf{p}_2 \mid = \frac{(m_1 - E_4)^2 - \mathbf{p}_4^2}{2\,(m_1 - E_4 + \mid \mathbf{p}_4 \mid \cos\theta_{24})}\,. \tag{A.6}$$

(This is the only physical solution for all $\mid \mathbf{p}_4 \mid \in [0, \mid \mathbf{p}_4 \mid^{max}]$ and $\theta_{24} \in [0, \pi\,]$.)

With this kinematical setup the total decay rate becomes

$$W = \frac{G^2}{32}\,\frac{8\pi^2}{(2\pi)^5}\,\frac{1}{m_1}\int_0^{p_4^{max}} dp_4\,\frac{p_4^2}{E_4}\int_0^{\pi} d\theta_{24}\,\frac{\sin\theta_{24}\;\mid \mathbf{p}_2 \mid\;\mathcal{R}}{\mid \mathbf{p}_2 \mid + \mid \mathbf{p}_2 + \mathbf{p}_4 \mid + \mid \mathbf{p}_4 \mid \cos\theta_{24}} \tag{A.7}$$

We evaluated W numerically and obtained

$$W = G^2\,2.1115 \times 10^6\,\mathrm{MeV}^5\,. \tag{A.8}$$

This is to be compared with the highly nontrivial analytical result given in Eq. (2.57) of Ref. [52], which reads

$$W = G^2\,\frac{m_1^5}{192\,\pi^3}\left(1 - 8y + 8y^3 - y^4 - 12y^2\ln y\right) \tag{A.9}$$

($y \equiv \frac{m_4^2}{m_1^2}$) and is numerically fully equivalent to our result in (A.8). Note that we do not discuss here any radiative corrections, which are introduced in [52]. The lifetime of the muon is $\tau = (2.197 \pm 0.00004) \times\ 10^{-6}$ Sec.

Appendix B

Neutron Beta decay

The neutron beta decay process,

$$n \to p + e^- + \bar{\nu}_e \,,$$

is of fundamental importance for our understanding of weak processes involving nucleons. From the point of view of the modern gauge theory of electro-weak interactions it cannot be considered as a truly elementary reaction and should be studied with quark degrees of freedom. We decided to repeat the simple exercise of calculating the neutron lifetime for two main reasons; first, because it provides a first idea about the single nucleon weak charged current operator; and secondly, because one can learn how to treat the kinematics of three-particle decays. Additionally, we can test our *Mathematica*® [21] notebooks and significantly simplify the calculations.

Our starting point to calculate the total free neutron decay rate (the inverse of the free neutron lifetime) are again Eqs. (2.18) and (2.19a) from [52], although they are

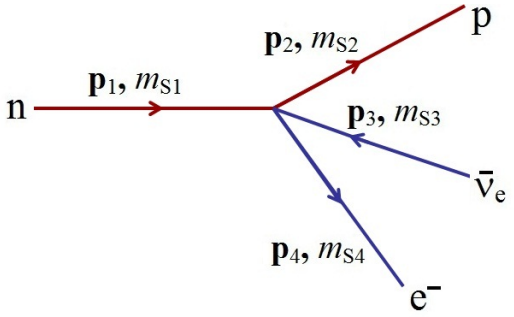

FIGURE B.1: Neutron beta decay diagram where $\mathbf{p}_i$, m_{s_i} is the three-momentum vector and the spin projection respectively.

originally given for the muon decay process:

$$W = \frac{G^2}{2}\,\frac{1}{(2\pi)^5}\,\frac{1}{2m_1}\int\frac{d^3p_2}{2E_2}\int\frac{d^3p_3}{2E_3}\int\frac{d^3p_4}{2E_4}$$
$$\delta^4\left(\tilde{p}_2+\tilde{p}_3+\tilde{p}_4-\tilde{p}_1\right)\,\frac{1}{2}\sum_{m_{s_1},m_{s_2},m_{s_3},m_{s_4}}\mid\widetilde{\mathcal{M}}\mid^2\ . \tag{B.1}$$

We deal in Eq. (B.1) with the four-momenta of the initial neutron at rest ($\tilde{p}_1 = (m_1, \mathbf{p}_1 = 0)$) and outgoing particles: the proton ($\tilde{p}_2 = (E_2, \mathbf{p}_2)$), the massless electron antineutrino ($\tilde{p}_3 = (E_3 =\mid \mathbf{p}_3 \mid, \mathbf{p}_3)$), and the electron ($\tilde{p}_4 = (E_4, \mathbf{p}_4)$). The quantity $\widetilde{\mathcal{M}}$ contains the essential information about the process and is given as a contraction of the nucleonic and leptonic parts [52]

$$\widetilde{\mathcal{M}} = \Big(\bar{u}(\mathbf{p}_2, m_{s_2})\gamma^\lambda(1-\bar{\alpha}\gamma_5)u(\mathbf{p}_1, m_{s_1})\Big)\Big(\bar{u}(\mathbf{p}_4, m_{s_4})\gamma_\lambda(1-\gamma_5)v(\mathbf{p}_3, m_{s_3})\Big)\,, \tag{B.2}$$

where the crucial parameter is $\bar{\alpha} \approx 1.3$. (Right here we replace the muonic part of Eq. (2.19a) from [52] by the nucleonic part given in Eq. (1.30) of the same reference.) In Eq. (B.1) we average over the initial neutron spin projections and sum over spin projections of the outgoing particles. Note that also in this appendix we use the spinor normalization of Ref. [52]. We expect that

$$\widetilde{\mathcal{R}} \equiv \frac{1}{2}\sum_{m_{s_1},m_{s_2},m_{s_3},m_{s_4}}\mid\widetilde{\mathcal{M}}\mid^2$$

is a scalar function and depends only on dot products of the momentum vectors of the three outgoing particles. Such quantities like $\widetilde{\mathcal{R}}$ are usually evaluated in a non-trivial way using various trace identities for the gamma matrices (see for example Ref. [23]). However, with the help *Mathematica*® [21] we easily arrive at the following formula:

$$\begin{aligned}
\widetilde{\mathcal{R}} = {}& 16\,\frac{m_1}{W_2}\,(\bar{\alpha}^2-1)\,\mathbf{p}_2^2\,\mathbf{p}_3\cdot\mathbf{p}_4\\
&-16\,\frac{m_1}{W_4}\,(\bar{\alpha}-1)^2\,\mathbf{p}_2\cdot\mathbf{p}_3\,\left(\mathbf{p}_4^2+W_4^2\right)\\
&-16\,m_1\,(\bar{\alpha}^2-1)\,\mathbf{p}_3\cdot\mathbf{p}_4\,W_2\\
&+8\,\frac{m_1}{W_2\,W_4}\,(3+\bar{\alpha}^2)\,\mid\mathbf{p}_3\mid\,\mathbf{p}_2^2\,\left(\mathbf{p}_4^2+W_4^2\right)\\
&-32\,m_1\,(1+\bar{\alpha})^2\,\mid\mathbf{p}_3\mid\,\mathbf{p}_2\cdot\mathbf{p}_4\\
&+8\,\frac{m_1}{W_4}\,(1+3\bar{\alpha}^2)\,\mid\mathbf{p}_3\mid\,W_2\,\left(\mathbf{p}_4^2+W_4^2\right)\,,
\end{aligned} \tag{B.3}$$

where

$$W_i \equiv m_i + E_i \equiv m_i + \sqrt{m_i^2+\mathbf{p}_i^2}\,. \tag{B.4}$$

Having obtained this general result for $\widetilde{\mathcal{R}}$ in (B.3), we can now decide how to calculate the integrals in Eq. (B.1). For the same reasons as in Appendix A we are left with a two dimensional integral. However, different kinematical choices can be made and they are discussed in the following subsections.

B.0.1 Kinematics 1

The proton-neutron mass difference is very small (approximately 1.3 MeV) so the kinetic energy of the emerging proton can be (at first at least) neglected compared to its mass. This suggests the following kinematical choice:

$$\begin{aligned} \mathbf{p}_1 &= (0,0,0)\,, \\ \mathbf{p}_2 &= (0,0,0)\,, \\ \mathbf{p}_4 = (0,0,\mid \mathbf{p}_4 \mid)\,, \qquad &\mid \mathbf{p}_4 \mid \in [0, \mid \mathbf{p}_4 \mid^{max}]\,, \\ \mathbf{p}_3 = (\mid \mathbf{p}_3 \mid \sin\theta_{34}, 0, &\mid \mathbf{p}_3 \mid \cos\theta_{34})\,, \end{aligned} \tag{B.5}$$

where

$$\mid \mathbf{p}_3 \mid = m_1 - m_2 - E_4 \tag{B.6}$$

and

$$\mid \mathbf{p}_4 \mid^{max} = \sqrt{(m_1 - m_2)^2 - m_4^2}\,. \tag{B.7}$$

With this kinematical setup $\widetilde{\mathcal{R}}$ is particularly simple:

$$\widetilde{\mathcal{R}} = 32 m_1 m_2 \mid \mathbf{p}_3 \mid \Big((1+3\bar{\alpha}^2) E_4 \; - \; (\bar{\alpha}^2 - 1) \mid \mathbf{p}_4 \mid \cos\theta_{34} \Big) \tag{B.8}$$

and the total decay rate becomes

$$\begin{aligned} W = \frac{G^2}{4\pi^3} \int_0^{p_4^{max}} dp_4 \, \frac{p_4^2}{E_4} \int_0^{\pi} d\theta_{34} \sin\theta_{34} \, (m_1 - m_2 - E_4) \\ \Big((1+3\bar{\alpha}^2) E_4 \; - \; (\bar{\alpha}^2 - 1) \mid \mathbf{p}_4 \mid \cos\theta_{34} \Big) \end{aligned} \tag{B.9}$$

The calculated lifetime $\tau_n = \frac{1}{W}$ is 878.34 Sec.

B.0.2 Kinematics 2

This kinematical choice is very similar to the one in subsection B.0.1 but we do not assume that the final proton is at rest and express its momentum as

$$\mathbf{p}_2 = -\mathbf{p}_3 - \mathbf{p}_4\,, \tag{B.10}$$

so the proton total energy E_2 is now given as

$$E_2 = \sqrt{m_2^2 + \mathbf{p}_3^2 + \mathbf{p}_4^2 + 2 \mid \mathbf{p}_3 \mid \mid \mathbf{p}_4 \mid \cos\theta_{34}}\,. \tag{B.11}$$

Standard steps lead then to the following formula for W:

$$W = \frac{G^2}{32}\,\frac{8\pi^2}{(2\pi)^5}\,\frac{1}{m_1}\int\limits_0^{p_4^{max}} dp_4\,\frac{p_4^2}{E_4}\int\limits_0^{\pi} d\theta_{34}\sin\theta_{34}\,\frac{\mid \mathbf{p}_3 \mid}{E_2}\,\frac{1}{\left|1+\frac{|\mathbf{p}_3|+p_4\cos\theta_{34}}{E_2}\right|}\,\widetilde{\mathcal{R}}\big(\mathrm{k}inematics\ 2\big)\,. \tag{B.12}$$

Here, however,

$$\begin{aligned} \mid \mathbf{p}_4 \mid^{max} &= \sqrt{\frac{\left(m_1^2 - m_2^2 + m_4^2\right)^2}{4m_1^2} - m_4^2}\,, \\ \mid \mathbf{p}_3 \mid &= \frac{-(m_1 - E_4)^2 + m_2^2 + p_4^2}{2\left(E_4 - m_1 - p_4\cos\theta_{34}\right)}\,. \end{aligned} \tag{B.13}$$

It is found the lifetime is about $\tau_N = 880.17$ Sec.

B.0.3 Kinematics 3

The kinematical choice presented in the previous subsection (and its simplified version from subsection B.0.1) has a very important feature: a simple rectangular region of integration. In this subsection we test yet another possibility, aiming at the kinematics, where the three-momentum transfer from the neutron to proton is parallel to the z axis. Such a choice is often dictated by the fact that calculations of the nuclear current matrix elements, especially in partial wave decomposition, are easiest in this case.

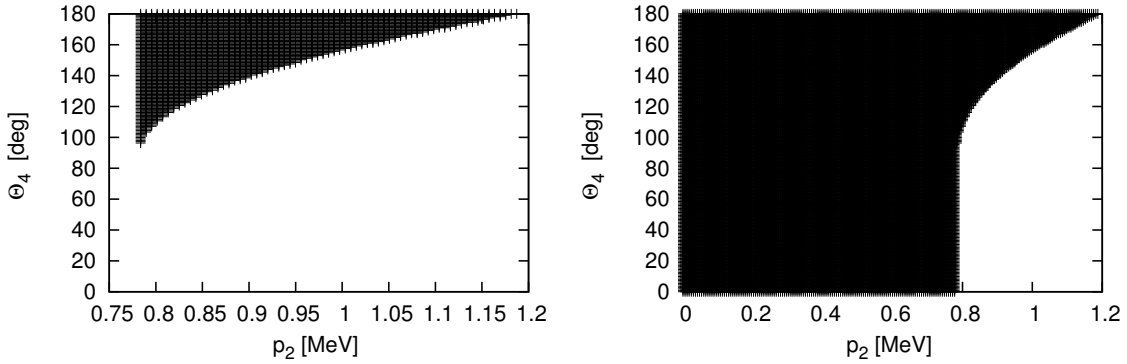

FIGURE B.2: The region of integration for the neutron beta decay process and kinematics 3 in the $p_2 - \theta_4$ plane. (see text)

Thus we set

$$\begin{aligned} \mathbf{p}_1 &= (0,0,0)\,, \\ \mathbf{p}_2 = (0,0,\mid \mathbf{p}_2 \mid)\,, \qquad \mid \mathbf{p}_2 \mid &\in [0,\mid \mathbf{p}_2 \mid^{max}]\,, \\ \mathbf{p}_4 &= (\mid \mathbf{p}_4 \mid \sin\theta_4, 0, \mid \mathbf{p}_4 \mid \cos\theta_4)\,, \\ \mathbf{p}_3 &= -\mathbf{p}_2 - \mathbf{p}_4\,, \end{aligned} \tag{B.14}$$

where

$$\mid \mathbf{p}_2 \mid^{max} = \sqrt{\frac{\left(m_1^2 + m_2^2 - m_4^2\right)^2}{4m_1^2} - m_2^2} \tag{B.15}$$

and $\mid \mathbf{p}_4 \mid$ is the physical (positive) solution to

$$m_1 = E_2 + \sqrt{\mathbf{p}_2^2 + \mathbf{p}_4^2 + 2 \mid \mathbf{p}_2 \mid \mid \mathbf{p}_4 \mid \cos\theta_4} + \sqrt{m_4^2 + \mathbf{p}_4^2}\,. \tag{B.16}$$

For this kinematical choice the total decay rate is given as

$$\begin{aligned} W = \frac{G^2}{32}\,\frac{8\pi^2}{(2\pi)^5}\,\frac{1}{m_1} \int_0^{p_2^{max}} dp_2\,\frac{p_2^2}{E_2} \int_{\theta_4^{min}}^{\theta_4^{max}} d\theta_4 \sin\theta_4 \\ \sum_i \left(\frac{\mathbf{p}_4^2}{\mid \mathbf{p}_3 \mid \; E_4}\,\frac{\widetilde{\mathcal{R}}\big(kinematics\ 3\big)}{\Big|(m_1 - E_2) \mid \mathbf{p}_4 \mid + E_4\, p_2 \cos\theta_4\Big|} \right). \end{aligned} \tag{B.17}$$

Note that in Eq. (B.17) we sum over i physical solutions of Eq. (B.16). The lifetime calculated by this kinematics is $\tau_n = 879.51$ Sec.

Appendix C

Schrödinger equation for the deuteron

In this appendix we explain how we solve the non-relativistic Schrödinger equation for the deuteron bound state,

$$H\ |\Psi_{deut} m_d\rangle \equiv (H_0 + V)\ |\Psi_{deut} m_d\rangle = E_{deut}\ |\Psi_{deut} m_d\rangle\,. \tag{C.1}$$

We work in the momentum space and employ the partial wave representation, so the deuteron is represented by its two components: the S-component with the orbital angular momentum $l = 0$ ($\varphi_0(p)$) and D-component with the orbital angular momentum $l = 2$ ($\varphi_2(p)$). We use the fact that only two basis states with the two-nucleon spin $s = 1$, total angular momentum $j = 1$ and the total isospin $t = 0$ contribute to the deuteron state and adopt a simplified notation

$$|pl\rangle \equiv |p(l1)1\rangle\ |00\rangle\,. \tag{C.2}$$

Since the deuteron wave function does not depend on the projection of the total angular momentum, m_d, we skip m_d in the following considerations. By projecting from the left with $\langle pl|$ Eq. (C.1) reads

$$\frac{p^2}{M_N}\varphi_l(p) + \sum_{l',l=0,2}\int dp' p'^2 \langle pl|V|p'l'\rangle\ \varphi_{l'}(p') = E_{deut}\ \varphi_l(p)\,, \tag{C.3}$$

where $\varphi_l(p) \equiv \langle pl|\Psi_{deut}\rangle$. For a numerical treatment of Eq. (C.3) we assume that the integral over p' is carried out with some choice of Gaussian points and weights (p_j, w_j) with $j = 1, 2, ..., N_P$ distributed in the finite interval $(0, \bar{p})$, where the upper limit of the integration, $\bar{p}$, might depend on the nucleon-nucleon potential used. For example, for all

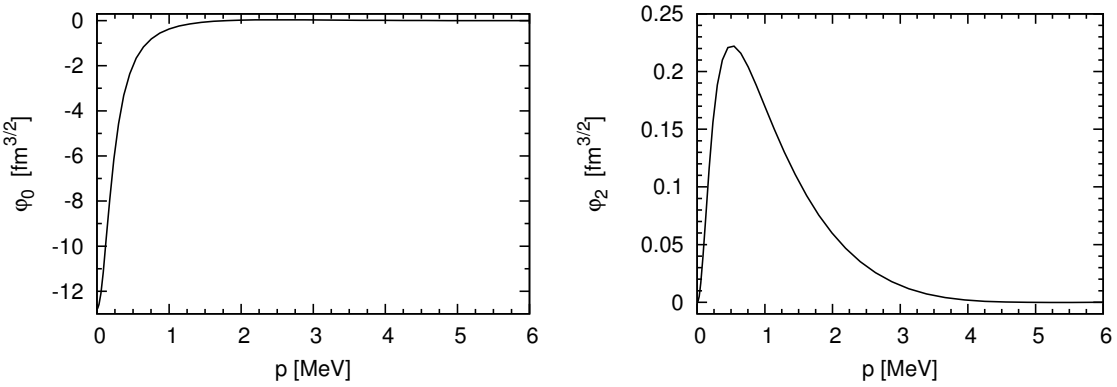

FIGURE C.1: The two deuteron components: $\varphi_0(p)$ (left) and $\varphi_2(p)$ (right) calculated using the improved N4LO chiral potential [18] with R= 1 fm as a function of the magnitude of the relative momentum p.

the improved chiral potentials [18] we take $N_P = 72$ Gaussian points up to $\bar{p} = 25$ fm^{-1}. As an intermediate step we obtain

$$\frac{p_i^2}{M_n}\varphi_l(p_i) + \sum_{l'=0,2}\sum_{j=1}^{N_P} w_j p_j^2 \langle p_i l|V|p_j l'\rangle \varphi_{l'}(p_j) = E_{deut}\ \varphi_l(p_i),\ l = 0, 2\,, \tag{C.4}$$

what can be written as an eigenvalue problem: $A\xi = E_{deut}\xi$. The components of the $2N_P$ dimensional vector ξ and of the $2N_P \times 2N_P$ matrix A are given as

$$\begin{aligned} \xi_i + \frac{1}{2}N_P &= \varphi_l(p_i), \\ A(i + \frac{l}{2}N_p, j + \frac{l'}{2}N_p) &= \delta_{ij}\ \delta_{ll'}\frac{p_i^2}{M_n} + w_i p_i^2 \langle p_i l|V|p_j l'\rangle, \\ i = 1, ..., N_P, \quad j = 1, ..., N_P, \quad l, l' &= 0, 2. \end{aligned} \tag{C.5}$$

We use the eigenproblem routines from the LAPACK library [53] to find the deuteron components $\varphi_l(p)$. Alternatively, we import the A matrix into *Mathematica*® [21] and use its *Eigensystem* function. Finally, the components are normalized as

$$\int_0^{\bar{p}} dp\ p^2\ (\varphi_0^2(p) + \varphi_2^2(p)) = 1\,. \tag{C.6}$$

In Fig. C.1 we show the two deuteron components calculated using the improved N4LO chiral potential [18] with R= 1 fm. The results for the lower orders of the chiral expansion and other regulators look similar.

Appendix D

Numerical solutions of the Lippmann-Schwinger equation

For the calculation of the nuclear matrix elements for the $\mu^- + d \to \nu_\mu + n + n$ reaction given in Eq. (3.6), we need the half-shell elements of the t-matrix,

$$\langle p_0 \alpha_2 | t(\frac{p^2}{M_N} + i\epsilon) | p_0' \alpha_2' \rangle \,, \tag{D.1}$$

where the magnitude of the final momentum p_0 is determined by the escaping muon neutrino energy. Due to the rotational invariance, parity conservation, spin and isospin conservation of the nucleon-nucleon potential these matrix elements may be written as

$$\Big\langle p_0(ls)jm_j; tm_t \Big| t(\frac{p_0^2}{M_N} + i\epsilon) \Big| p'(l's')j'm_j'; t'm_t' \Big\rangle =$$
$$\delta_{j,j'}\, \delta_{m_j,m_j'}\, \delta_{(-1)^l,(-1)^{l'}}\, \delta s, s'\, \delta_{t,t'}\, \delta_{m_t,m_t'} \Big\langle p_0(ls)j; t | t(\frac{p_0^2}{M_N} + i\epsilon) | p'(l's')j; t \Big\rangle, \tag{D.2}$$

which means that either $l = l'$ (uncoupled channel) or $l - l' = \pm 2$ (two coupled channels). We show how the Lippmann-Schwinger equation

$$t = V + tG_0V \tag{D.3}$$

is solved numerically for the more difficult case of two coupled channels, which occurs for $j > 0$ only if $s = 1$. Using a shorthand notation

$$\langle p_0 l | t | p' l' \rangle \equiv \langle p_0 \alpha_2 | t | p' \alpha_2' \rangle \,, \tag{D.4}$$

The partial-wave projected Eq. (D.3) takes the following form:

$$\langle p_0 l|t|p' l'\rangle = \langle p_0 l|V|p' l'\rangle + \sum_{l''=j-1,j+1} \int_0^{\bar{p}} dp'' \frac{p''^2 \langle p_0 l|t|p'' l''\rangle \ \langle p'' l''|V|p' l'\rangle}{\frac{p_0^2}{M_N} - \frac{p''^2}{M_N} + i\epsilon} \tag{D.5}$$

with $\epsilon \to 0^+$. Treating the singularity by subtraction we obtain

$$\begin{aligned} \langle p_0 l|t|p' l'\rangle &= \langle p_0 l|V|p' l'\rangle \\ &+ M_N \sum_{l''} \int_0^{\bar{p}} dp'' \frac{p''^2 \langle p_0 l|t|p'' l''\rangle \ \langle p'' l''|V|p' l'\rangle - p_0^2 \langle p_0 l|t|p_0 l''\rangle \ \langle p_0 l''|V|p' l'\rangle}{p_0^2 - p''^2} \\ &+ \frac{M_N p_0}{2} \Big[\ln \Big| \frac{\bar{p} + p_0}{\bar{p} - p_0} \Big| - i\pi \Big] \ \sum_{l''} \langle p_0 l|t|p_0 l''\rangle \ \langle p_0 l''|V|p' l'\rangle \,, \end{aligned} \tag{D.6}$$

where we use the following formula

$$\lim_{\epsilon \to 0^+} \int_0^{\bar{p}} \frac{dp}{p_0^2 - p^2 + i\epsilon} = \frac{1}{2p_0} \Big[\ln \Big| \frac{\bar{p} + p_0}{\bar{p} - p_0} \Big| - i\pi \Big]. \tag{D.7}$$

Here again we choose a set of Gaussian points and weights (p_n, w_n) with $n = 1, 2, ..., N_P$ given on the interval $(0, \bar{p})$. We supplement this set with an additional pair $(p_0, w_0 = 0)$ and require that $p_n \neq p_0$ for $n > 1$. This is done because in Eq. (D.6) we need also $\langle p_0 l|t|p_0 l''\rangle$. Both the upper limit $\bar{p}$ and the number of integral points N_P must be chosen in a way which yields stable results. With

$$\begin{aligned} Z &\equiv \frac{M_N p_0}{2} \Big[\ln \Big| \frac{\bar{p} + p_0}{\bar{p} - p_0} \Big| - i\pi \Big], \\ H &\equiv M_N p_0^2 \sum_{n=1}^{N} \frac{w_n}{p_0^2 - p_n^2}, \\ \tilde{w}_n &\equiv \begin{cases} 0 & , \ n=0 \\ \frac{M_N w_n p_n^2}{p_0^2 - p_n^2} & , \ n \neq 0 \end{cases} \end{aligned} \tag{D.8}$$

We obtain a set of $2(N_P + 1)$ algebraic equations

$$\begin{aligned} &\sum_{l''} \sum_{n=0}^{N_P} [\tilde{w}_n \langle p_n l''|V|p_i l'\rangle - H \langle p_0 l''|V|p_i l'\rangle \delta_{n0} \\ &+ Z \langle p_0 l''|V|p_i l'\rangle \delta_{n0} - \delta_{in} \delta_{l' l''} \ ] \langle p_0 l|t|p_n l''\rangle = -\langle p_0 l|V|p_i l'\rangle \end{aligned} \tag{D.9}$$

for $2(N_P + 1)$ unknown matrix elements $\langle p_0 l|t|p_n l''\rangle$, which we solve separately for each l. To be explicit, we write it as

$$\sum_d A_{kd} \xi_d = B_k \,, \tag{D.10}$$

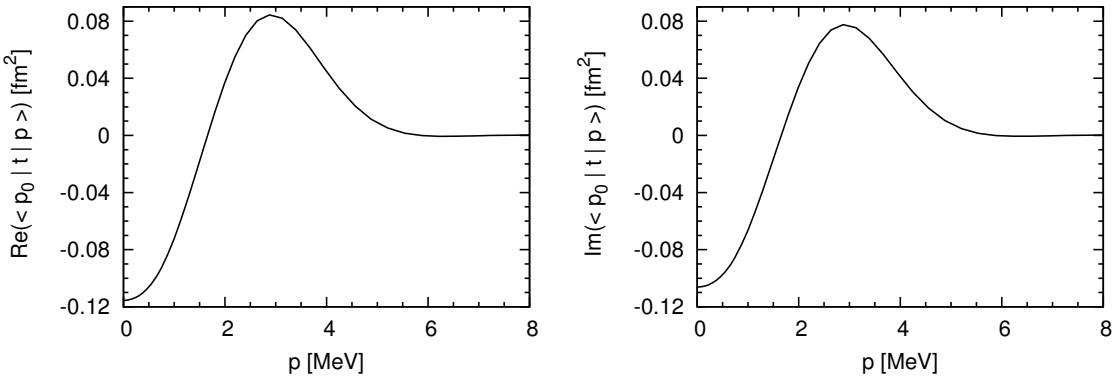

FIGURE D.1: The real (left) and imaginary (right) part of the half-shell t-matrix $\langle p_0|t\left(\frac{p_0^2}{M}|p\rangle\right)$ for the ${}^1S_0$ partial wave calculated using the improved N4LO chiral potential [18] with R= 1 fm as a function of the initial momentum p. The final momentum p_0= 0.69 fm^{-1}.

where

$$
\begin{aligned}
l, l', l'' &= j-1, j+1, \\
k = i+1+\frac{l'-j+1}{2}(N_P+1),\ & i = 0,1,2,....,N_P, \\
d = n+1+\frac{l''-j+1}{2}(N_P+1),\ & n = 0,1,2,....,N_P, \\
\xi_d &\equiv \langle p_0 l|t|p_n l''\rangle, \\
b_k &\equiv -\langle p_0 l|t|p_i l'\rangle, \\
A_{kd} \equiv \tilde{w}_n\langle p_0 l''|V|p_i l'\rangle &+ (Z-H)\langle p_0 l''|V|p_i l'\rangle\delta_{n0} - \delta_{in}\delta_{l'l''}
\end{aligned}
\tag{D.11}
$$

We solve this system of equations numerically using the standard LU decomposition routines from the LAPACK library [53]. The case of the uncoupled channel is simpler, since $l = l' = l''$ and we deal with a system of $N_P + 1$ coupled equation for unknown $\langle p_0 l|T|p_n l\rangle$ matrix elements. We show just one example in Fig. D.1, where we choose the dominant ${}^1S_0$ partial wave and p_0= 0.69 fm^{-1}. The Lippmann-Schwinger equation is solved using the improved N4LO chiral potential [18] and the R= 1 fm regulator. It is quite surprising that the real and imaginary parts of the selected matrix elements look nearly the same.

Bibliography

[1] A. Pais, *Inward Bound: Of Matter and Forces in the Physical World*, Oxford University Press, New York, 1986.

[2] A. Lesov, arXiv:0911.0058 [physics.hist-ph] (2009).

[3] G. Rajasekaran, arXiv:1403.3309 [physics.hist-ph] (2014); Resonance (Indian Academy of Sciences, Bangalore), Vol 19, No 1, pp. 18-44, January 2014.

[4] V.A. Andreev *et al.*, arcXiv: 1004.1754 [nuclex] (2010); see also the web page of the MuSun experiment:
http://muon.npl.washington.edu/exp/MuSun/

[5] D.F. Measday, Phys. Rep. **354**, 243 (2001).

[6] T. Gorringe and H.W. Fearing, Rev. Mod. Phys. **76**, 31 (2004).

[7] P. Kammel and K. Kubodera, Annu. Rev. Nucl. Part. Sci. **60**, 327 (2010).

[8] L. E. Marcucci, M. Piarulli, M. Viviani, L. Girlanda, A. Kievsky, S. Rosati, and R. Schiavilla, Phys. Rev. C **83**, 014002 (2011).

[9] L.E. Marcucci, Int. J. Mod. Phys. A **27** 1230006 (2012).

[10] L.E. Marcucci, R, Schiavilla, S. Rosati, A. Kievsky, and M. Viviani, Phys. Rev. C **66**, 054003 (2002).

[11] L.E. Marcucci, R. Schiavilla, M. Viviani, A. Kievsky, S. Rosati, and J.F. Beacom, Phys. Rev. C **63**, 015801 (2000).

[12] L.E. Marcucci, A. Kievsky, S. Rosati, R. Schiavilla, and M. Viviani, Phys. Rev. Lett. **108**, 052502 (2012).

[13] R. Skibiński, J. Golak, H. Witała, and W. Glöckle, Phys. Rev. C**59**, 2384 (1999).

[14] J. Golak, R. Skibiński, H. Witała, K. Topolnicki, A. E. Elmeshneb, H. Kamada, A. Nogga, L. E. Marcucci, Phys. Rev. C **90**, 024001 (2014).

[15] J. Golak, R. Skibiński, H. Witała, W. Glöckle, A. Nogga, and H. Kamada, Phys. Rept. **415**, 89 (2005).

[16] R. Skibiński, J. Golak, H. Witała, W. Glöckle, and A. Nogga, Eur. Phys. J. A **24**, 31-38 (2005).

[17] A. Kievsky, S. Rosati, M. Viviani, L.E. Marcucci, and L. Girlanda, J. Phys. G **35**, 063101 (2008).

[18] E. Epelbaum, H. Krebs, U.-G. Meißner, arXiv:1412.0142 [nucl-th] (2014).

[19] R.B. Wiringa, V.G.J. Stoks, and R. Schiavilla, Phys. Rev. C **51**, 38 (1995).

[20] B.S. Pudliner, V.R. Pandharipande, J. Carlson, Steven C. Pieper, and R.B. Wiringa, Phys. Rev. C **56**, 1720 (1997).

[21] Wolfram Research, Inc., *Mathematica*®, Version 9.0, Champaign, IL (2012).

[22] J.D. Walecka, *Theoretical Nuclear and Subnuclear Physics*, Oxford University Press, New York, 1995.

[23] J.D. Bjorken, S.D. Drell, *Relativistic Quantum Mechanics*, McGraw-Hill Science/Engineering/Math, 1998.

[24] D. Bailin, *Weak interactions*, Adam Hilger, Bristol, 1982.

[25] G. Shen, L.E. Marcucci, J. Carlson, S. Gandolfi, and R. Schiavilla, Phys. Rev. C **86** 035503 (2012).

[26] J. Golak, D. Rozpędzik, R. Skibiński, K. Topolnicki, H. Witała, W. Glöckle, A. Nogga, E. Epelbaum, H. Kamada, Ch. Elster, and I. Fachruddin, Eur. Phys. J. A **43**, 241 (2010).

[27] R. Skibiński, J. Golak, K. Topolnicki, H. Witała, H. Kamada, W. Glöckle, and A. Nogga, Eur. Phys. J. A **47**, 48 (2011).

[28] D. Rozpędzik, PhD thesis, Jagiellonian University (unpublished), 2010.

[29] D. Rozpędzik, J. Golak, S. Kölling, E. Epelbaum, R. Skibiński, H. Witała, and H. Krebs, Phys. Rev. C **83**, 064004 (2011).

[30] B. H. Bransden and C. J. Joachain, *Physics of Atoms and Molecules*, Longman Scientific & Technical, 1983.

[31] R. Machleidt, Adv. Nucl. Phys. **19**, 189 (1989).

[32] E. Epelbaum, W. Glöckle, and U.-G. Meißner, Nucl. Phys. A **747**, 362 (2005).

[33] I.-T. Wang *et al.*, Phys. Rev. **139**, B1528 (1965).

[34] A. Bertin *et al.*, Phys. Rev. D **8**, 3774 (1973).

[35] G. Bardin *et al.*, Nucl. Phys. A **453**, 591 (1986).

[36] M. Cargnelli *et al.*, *Workshop on fundamental μ physics*, Los Alamos, 1986, LA 10714C; *Nuclear Weak Process and Nuclear Structure, Yamada Conference XXIII*, ed. M. Morita, H. Ejiri, H. Ohtsubo, and T. Sato (Word Scientific, Singapore), p. 115 (1989).

[37] K. Topolnicki, J. Golak, R. Skibiński, A.E. Elmeshneb, W. Glöckle, A. Nogga, and H. Kamada, Few-Body Syst. **54**, 2223 (2013).

[38] L. E. Marcucci, private communication.

[39] M. Bosman *et al.*, Phys. Lett. 82B, 212 (1979).

[40] Y. Birenbaum, S. Kahane, R. Moreh, Phys. Rev. C **32**, 1825 (1985).

[41] R. Bernabei *et al.*, Phys. Rev. Lett. **57**, 1542 (1986).

[42] R. Moreh, T. J. Kennett, and W. V. Prestwich, Phys. Rev. C **39**, 1247 (1989); Erratum: Phys. Rev. C **40**, 1548 (1989).

[43] A. Nogga, private communication.

[44] P. Ackerbauer *et al.*, Phys. Lett. B **417**, 224 (1998).

[45] A.F. Yano, Phys. Rev. Lett. **12**, 110 (1964).

[46] A.C. Philips, F. Roig, and J. Ros, Nucl. Phys. A **237**, 493 (1975).

[47] J.G. Congleton, Nucl. Phys. A **570**, 511 (1994).

[48] O.A. Zaĭmidoroga *et al.*, Phys. Lett. **6**, 100 (1963).

[49] L.B. Auerbach *et al.*, Phys. Rev. **138**, B127 (1965).

[50] E.M. Maev *et al.*, Hyp. Interact. **101/102**, 423 (1996).

[51] V.M. Bystritsky, V.F. Boreiko, M. Filipowicz, V.V. Gerasimov, O. Huot, P.E. Knowles, F. Mulhauser, V.N. Pavlov, L.A. Schaller, H. Schneuwly, V.G. Sandukovsky, V.A. Stolupin, V.P. Volnykh, and J. Woźniak, Phys. Rev. A **69**, 012712 (2004).

[52] W. Greiner, B. Müller, *Gauge Theory of Weak Interactions*, 3rd Ed., Springer, 2009.

[53] LAPACK-The Linear Algebra PACKage; http://www.netlib.org/lapack/index.html